A statistical study of large-amplitude parallel electric fields in the upward current region of the auroral acceleration region

A. J. Hull, J. W. Bonnell, and F. S. Mozer
Space Sciences Laboratory, University of California, Berkeley, California, USA

J. D. Scudder
Department of Physics and Astronomy, University of Iowa, Iowa City, Iowa, USA

Received 6 July 2001; revised 26 December 2001; accepted 10 May 2002; published XX Month 2002.

[1] We present a survey of 64 direct observations of large-amplitude parallel electric fields $E_{\|}$ in the upward current region of the southern auroral acceleration zone, obtained by the three-axis electric field experiment on Polar. These $E_{\|}$ events range in amplitude from about 25 to 300 mV/m and represent a significant fraction of the total electric field strength ($E_{\|}/E_{\perp}$ ranges from ~0.25 to O(10)). The $E_{\|}$ structures, which tend to occur at the edges of oppositely directed (converging) pairs of perpendicular electric field structures (electrostatic shocks), have transverse (to the magnetic field) widths of ~1.0–20 km at altitudes ranging from $0.8R_E$ to $1.5R_E$, assuming the structures are stationary. The parallel potential drops associated with these large-amplitude parallel electric fields are highly localized in altitude (e.g., tens of kilometers as opposed to ~thousands of kilometers). The amplitude of the parallel electric field shows a strong anticorrelation with the plasma density inferred from spacecraft potential measurements. We find no apparent correlation between the amplitude of the parallel electric field and altitudes sampled (between $0.8R_E$ and $1.5R_E$), current density, and K_p, though there is a suggestion that the largest $E_{\|}/E_{\perp}$ ratios are confined to lower altitudes. Taking sampling biases into consideration, we find that the large parallel electric fields occur preferentially at higher values of K_p and within a thin layer centered about $1.28R_E$. A detailed analysis favors ambipolar effects over electron inertial effects as an explanation for the parallel electric field signatures. *INDEX TERMS:* 2704 Magnetospheric Physics: Auroral phenomena (2407); 2712 Magnetospheric Physics: Electric fields (2411); 2736 Magnetospheric Physics: Magnetosphere/ionosphere interactions

Citation: Hull, A. J., J. W. Bonnell, F. S. Mozer, and J. D. Scudder, A statistical study of large-amplitude parallel electric fields in the upward current region of the auroral acceleration region, *J. Geophys. Res.*, *107*(0), XXXX, doi:10.1029/2001JA007540, 2002.

1. Introduction

[2] Electric fields parallel to the magnetic field vector play a major role in the transport of mass, momentum, and energy in the auroral zone. In the upward current region, higher altitude, large-amplitude perpendicular electric fields $E_{\perp}$ are prevented from mapping to the ionosphere via a parallel electric field $E_{\|}$. The $E_{\|}$ is of a sense to accelerate ions of ionospheric origin upwards and magnetospheric electrons downward, maintaining current and quasineutrality in the presence of a mirroring magnetic field. The parallel potential drop experienced by the particles typically ranges from 1 to 10 kV. Although localized in latitude, the parallel potential is usually envisioned to be distributed over a large altitude extent (~ thousands of kilometers), giving rise to a relatively small amplitude $E_{\|}$ (~ few mV/m) throughout the acceleration region.

[3] The generally accepted model of the canonical U-shaped potential well is depicted in Figure 1a, as a reference.

0148-0227/02/2001JA007540$09.00

[4] Large-amplitude, transient (AC) parallel electric fields associated with ion acoustic waves [e.g., *Ergun et al.*, 1998a] and solitary structures have been observed in the auroral acceleration region [e.g., *Temerin et al.*, 1982; *Ergun et al.*, 1998b; *Cattell et al.*, 1999]. It is not clear what role, if any, these large-amplitude AC parallel fields play in the formation of a quasistatic parallel potential drop in the acceleration region. Large-amplitude, macroscopic (DC) parallel electric fields were first encountered by S3-3 [e.g., *Mozer*, 1980; *Mozer et al.*, 1980] and more recently by Polar [*Mozer and Kletzing*, 1998; *Mozer and Hull*, 2001] and by FAST [*Ergun et al.*, 2001]. The few examples from Polar had amplitudes ranging from 200 to 300 mV/m and occurred in the upward current part of the southern auroral acceleration region at altitudes of about 6400 km on the boundary between high and low density plasma. Such large-amplitude DC parallel electric fields imply significant parallel potential drops distributed over tens of kilometers [*Mozer and Kletzing*, 1998], as opposed to potential drops distributed over thousands of kilometers. *Mozer and Hull* [2001] suggested that the large DC parallel electric fields are part of the field structure of the auroral acceleration

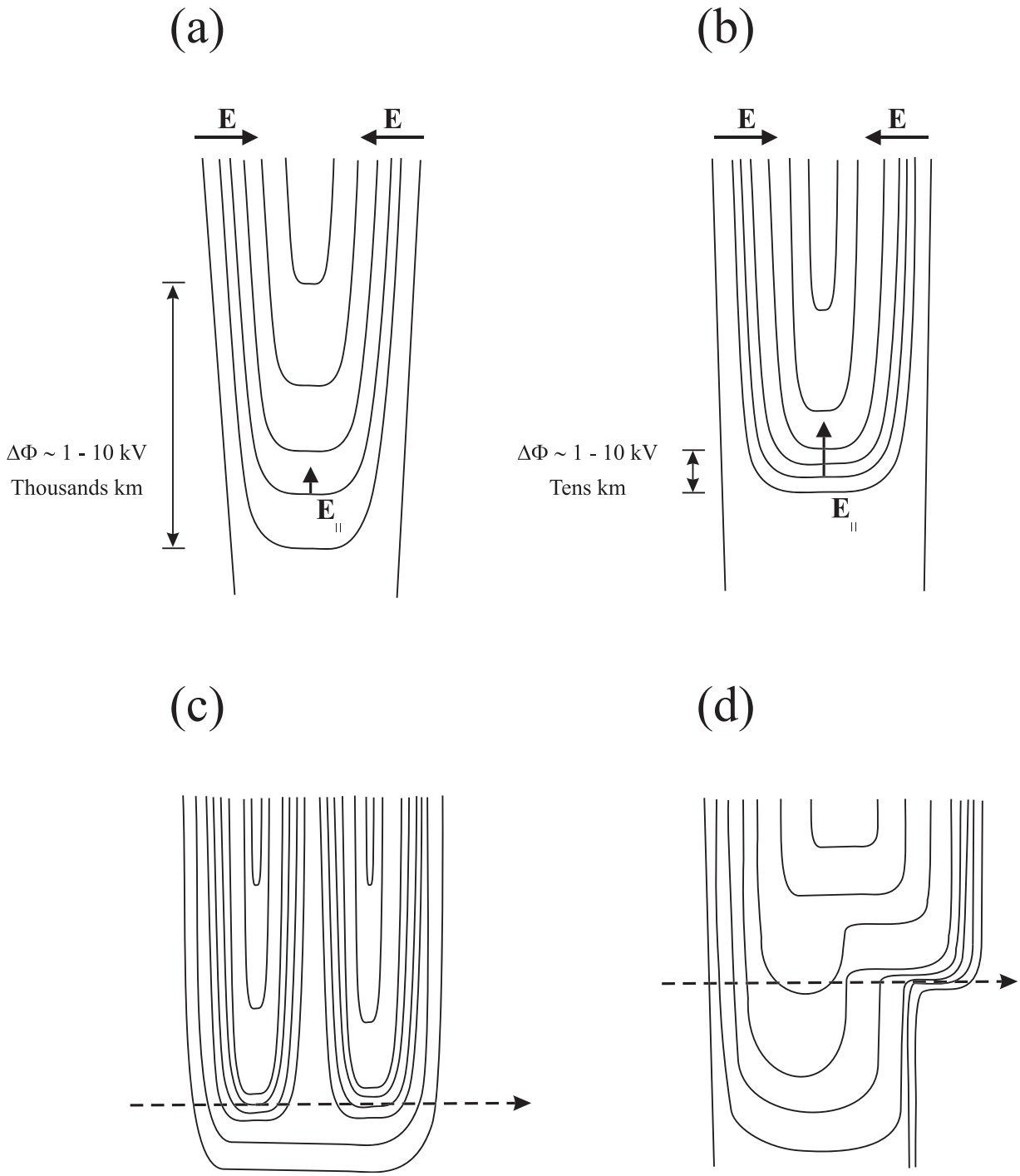

Figure 1. Quasistatic models of the potential along the field line inferred from the observations. The solid curves represent equipotential surfaces.

region and they occur in a sheath that separates the dense ionosphere from the less dense, higher altitude region. Figure 1b illustrates a revised U-shaped model of the potential well associated with the upward current part of the acceleration region envisioned by *Mozer and Hull* [2001]. Thus, in addition to weak parallel electric fields that exist at mid to high altitudes, the auroral acceleration region is envisioned to have strong, localized parallel electric fields at low altitudes. Highly localized, large-amplitude, DC parallel electric fields have also been suggested in recent simulations [*Ergun et al.*, 2000], although the simulated occurrence of the sharp transitions in potential along the field-line was sensitive to the boundary conditions imposed.

[5] It is not obvious whether localized DC parallel electric fields are a property of the typical state of the auroral acceleration region or arise under special circumstances. Statistical studies of direct measurements of DC parallel electric fields as a function of longitude, latitude, and altitude are essential to understanding the morphology

of the parallel potential, the mechanism(s) responsible for their formation, and their relation to particle acceleration. To date only a few examples of large-amplitude, macroscopic parallel electric fields exist in the literature. In this study we present a statistical survey of 64 large-amplitude, macroscopic parallel electric field structures measured in the southern auroral acceleration region by the three-axis electric field experiment on Polar at altitudes from $0.8R_E$ to 1.5 R_E. The $E_\parallel$ events have peak amplitudes ranging from 25 to 300 mV/m and represent a significant fraction of the total electric field strength ($E_\parallel/E_\perp$ range from $\sim$0.25 to O(10)). In section 3 we present a five case studies of $E_\parallel$ to illustrate some of their characteristic properties. Section 4 establishes the statistical properties of the $E_\parallel$ structures in relation to other parameters that characterize the auroral acceleration region. In section 5 we test the degree to which the large-amplitude DC parallel electric fields can be explained macroscopically by electron inertia and ambipolar effects. The ambipolar term of the generalized Ohm's law is found to be a plausible explanation for these large-amplitude DC parallel electric field signatures discussed in this paper, while the electron inertial term is not. Conclusions are given in section 6.

2. Instrumentation and Experimental Data Set

[6] The electric field data used in this study were measured by the electric field instrument (EFI) on board Polar [*Harvey et al.*, 1995]. EFI consists of three orthogonal sphere pairs that measure the electric field vector. The spin plane double probes have separations of 100 and 130 m, respectively. The third pair of spheres lie along the spin axis and are held 14 m apart by rigid booms. The electric field is regularly sampled at a rate of 40 vectors per second through a 20-Hz low-pass filter. Magnetic field data at 8 vectors per second were provided by the Polar magnetic field experiment (MFE) [*Russell et al.*, 1995]. Burst electric field data, sampled at 1600 Hz, were available for one of the events discussed in the paper. The burst electric field signals were low-pass filtered at 500 Hz. The search coil magnetic fields from PWI [*Gurnett et al.*, 1995] were sampled at the same rate as the burst electric field data.

[7] The electric field data used in this study are presented in a local magnetic field aligned coordinate (FAC) system in which the z axis represents the direction along the magnetic field, the x axis is in the magnetic meridional plane and points equatorward, and the y axis completes the orthonormal set and points in the magnetic westward direction. The 8-Hz magnetic field vector data were linearly interpolated to the electric field time tags before transforming the electric field vector from a despun spacecraft coordinate system into the FAC system.

[8] The high time resolution (1.15 s) electron and ion data used in this paper were measured by the DuoDeca Electron Ion Spectrometer (DDEIS) component of the Hydra instrument onboard Polar [*Scudder et al.*, 1995]. The DDEIS is composed of six pairs of E/Q analyzers which measure counts in 12 look directions with narrow fields of view ($8^\circ \times 8^\circ$) and energy bandwidth of $\Delta E/E = 6\%$, alternating between electron and ion samples in subsequent energy sweeps (1.15 s). Each sweep consists of 16 logarithmic energy steps from about 12 eV to 18 keV. Unless specifically stated otherwise, the electron and ion data used in this study have been corrected for spacecraft floating potential using direct measurements from EFI.

[9] All southern auroral zone passes from April 1996 to February 1999 were examined to find candidate events where large parallel electric fields were observed. We then imposed the following stringent criteria [see also *Mozer and Kletzing*, 1998] to remove all events that could be due to systematic or instrumental effects: (1) Sufficiently large electric fields can saturate the probe electronics, causing unphysical parallel electric field signals. Events affected by probe saturation were identified and removed from this data set. (2) Shadow effects, such as solar illumination or magnetic aspect, can produce spurious fields by modifying the floating potentials of the probes, therefore any event that showed any evidence of shadow effects was discarded. (3) Wake effects and high ambient plasma densities can produce spurious fields. Thus any event that showed evidence of wake effects (e.g., different estimates of the spacecraft potential from different pairs of probes; anomalous independent response of one or more of the probes) was discarded. (4) Electric fields are less accurately measured along the spin axis than in the spin plane because the spin axis booms are much shorter than the spin plane booms and because the spin axis electric field offsets are difficult to determine. Fortunately, Polar's spin plane is often nearly coplanar with the magnetic field vector, allowing for accurate measurement parallel electric field. Thus in this study, only events where the magnetic field was close (within 10 degrees) to the spin plane were considered. Each candidate event was manually inspected to make certain that the spin axis measurement did not influence the parallel field signature. We established the influence of the spin axis measurement on the parallel electric field component by comparing electric field measurements (including the contribution from the spin axis measurement) transformed to a field-aligned coordinate (FAC) system with FAC transformed measurements obtained under the assumption that the spin axis measurement is zero. Events shown to be significantly impacted by the spin axis measurement were discarded. (5) The spin plane electric field offsets are known with finite precision, leading to an error of a few mV/m in any spin plane electric field component. Thus any event where $E_\parallel$ was less than 25 mV/m was discarded. (6) The angular uncertainty in the magnetic field direction is known with finite precision. This uncertainty is typically much less than one degree but can, at times, be as much as a few degrees. Thus a spurious parallel electric field of up to $0.1E_\perp$ could be seen due to an error in the determination of the FAC system. Thus any event with $E_\parallel/E_\perp < 0.2$ was discarded. In addition, we discarded parallel electric field events which were significantly affected by arbitrary rotations of $\pm 5^\circ$ of the magnetic field direction. A detailed discussion on the validation of parallel electric fields observed by Polar based on these criteria is presented elsewhere (Scudder et al., submitted to *Journal of Geophysical Research*, 2001). Thus below we present the results of our analysis.

3. Case Studies of $E_\parallel$

[10] Three years of Polar EFI data from April 1996 to February 1999 yielded 64 events that satisfied our

selection criteria. In this section, we provide five events where large-amplitude, macroscopic parallel electric field structures were encountered by Polar in the southern auroral zone. The events chosen are representative of the $E_{\|}$ structures that make up our statistical database. We give evidence suggesting that the macroscopic parallel electric field structures, which are the focus of this paper, are different from the short duration, large-amplitude solitary structures previously reported in the literature [e.g., *Temerin et al.*, 1982; *Ergun et al.*, 1998b; *Cattell et al.*, 1999] or ion cyclotron wave fields [e.g., *Ergun et al.*, 1998a] with significant electric field component along the magnetic field vector. Moreover, we tested the kinetic Alfvén wave expectation of the parallel and perpendicular fields and demonstrated that at least for the example tested the explanation does not appear to be feasible.

3.1. 14 September 1996 Event

[11] An example of a southern auroral zone crossing on 14 September 1996 at an altitude of $\sim 1 R_E$ is illustrated in Figure 2. The three hour averaged K_p was 2+. Polar was near local noon at an invariant magnetic latitude $\sim 75°$, and with increasing time it moved poleward (toward higher invariant latitude) across a region of small amplitude electric fields to subsequently encounter a region containing large-amplitude electric field structures occurring after about 0622:10 UT (see Figures 2a–2c). Figures 2a–2c depict the 3 components of the electric field in the FAC system defined previously in section 2. It is important to note that the electric field range for Figure 2c is different from that of Figures 2a and 2b to make the parallel electric field component clearly visible. In Figure 2c, parallel electric fields ranging in amplitude from 70 to 35 mV/m are observed near 0622:13 UT and 0622:26 UT, respectively. The $E_{\|}$ events appear to occur between opposing (converging) pairs of large-amplitude perpendicular electric fields (see Figures 2a and 2b), which range in amplitude from 200 to 350 mV/m. The peak instantaneous $E_{\|}/E_{\perp}$ ratio for these events are found to be 15 and 10, respectively. Figure 2d depicts the negative of the spacecraft floating potential Φ_{SC}, which is a proxy for the plasma density [*Scudder et al.*, 2000]. Values of Φ_{SC} near zero correspond to high density plasma, whereas large negative values of Φ_{SC} correspond to low density plasma. In this example the density ranges from ~ 10 cm^{-3} in the low field regions to a minimum of ~ 0.1 cm^{-3} in the regions that correspond to large-amplitude electric field signatures. The east-west component of the magnetic field perturbation ΔB_Y is given in Figure 2e. The slope provides an estimate of the amplitude of the field-aligned current density, assuming the current structure is convecting by the spacecraft at the spacecraft speed. The decrease in ΔB_Y with increasing invariant magnetic latitude during the interval encompassing the $E_{\|}$ events ($\sim$0622:10 UT to 0622:50 UT) suggests that $E_{\|}$ occurred in a region of upward field aligned current. Figure 2f shows the plasma potential Φ_{pl}, which is determined by integrating $E_{\perp}$ along Polar's trajectory. The parameter Φ_{pl} is a measure of potential below Polar assuming a quasistatic potential model. Figure 2f suggests a ~ 1 kV parallel potential drop below the spacecraft during the $E_{\|}$ intervals.

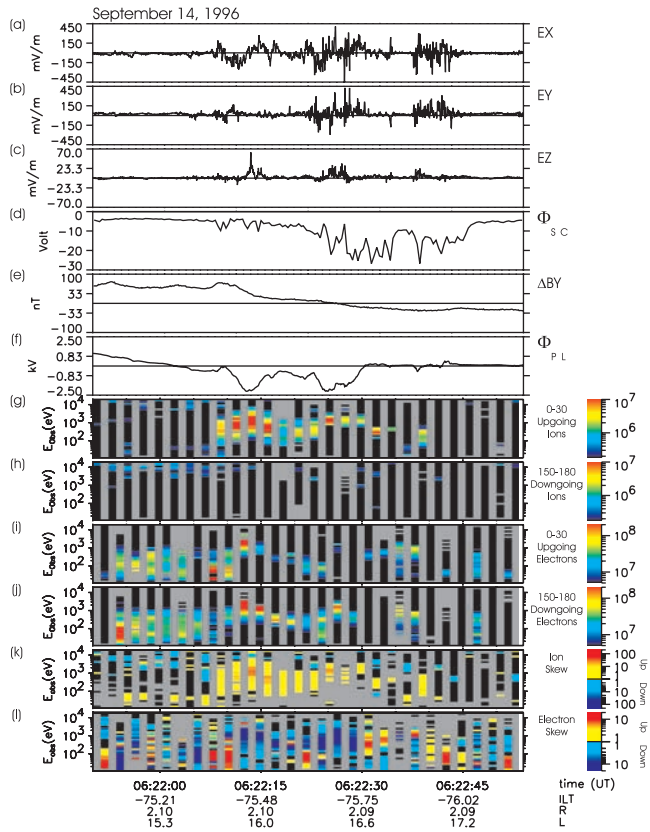

Figure 2. A southern auroral zone crossing near local noon on 14 September 1996. Shown are (a)–(c) the components of the electric field vector in field-aligned coordinates, (d) the spacecraft potential, (e) the east-west perturbation magnetic field, (f) the plasma potential, (g)–(h) spectrograms of the field-aligned and field-opposed differential ion energy flux, respectively, (i)–(j) spectrograms of the field-aligned and field-opposed differential electron energy flux, and spectrograms of the (k) ion skew and (l) electron skew.

[12] Spectrograms of ion differential energy flux for pitch angle ranges from 0° to 30° (upward) and 150° to 180° (downward) are depicted in Figures 2g and 2h, respectively. Similarly, electron spectrograms for pitch angle ranges from 0° to 30° and 150° to 180° are depicted in Figures 2i and 3j, respectively. Figures 2k and 2l display spectrograms of the ion and electron skew defined as the difference between the field-aligned and opposed differential energy fluxes normalized by the estimated systematic and statistical measurement uncertainty in that difference. Intense field-aligned ion beams with a mean energy of ~ 1 keV are shown to be concurrent with the large-amplitude parallel electric fields (see Figures 2g and 2h). The variation of ion beam energy is shown to be consistent with the variation of Φ_{pl} depicted in the Figure 2f. The predominance of the upgoing ion flux with respect to the downgoing flux is apparent from the yellow to orange enhancements in the ion skew displayed in Figure 2k from about 0622:10 to 0622:30 UT. Enhancements in the downgoing electron energy flux are observed simultaneously with the upgoing ion beams (Figure 2j). The blue in electron skew depicted in Figure 2l from 0622:10 to

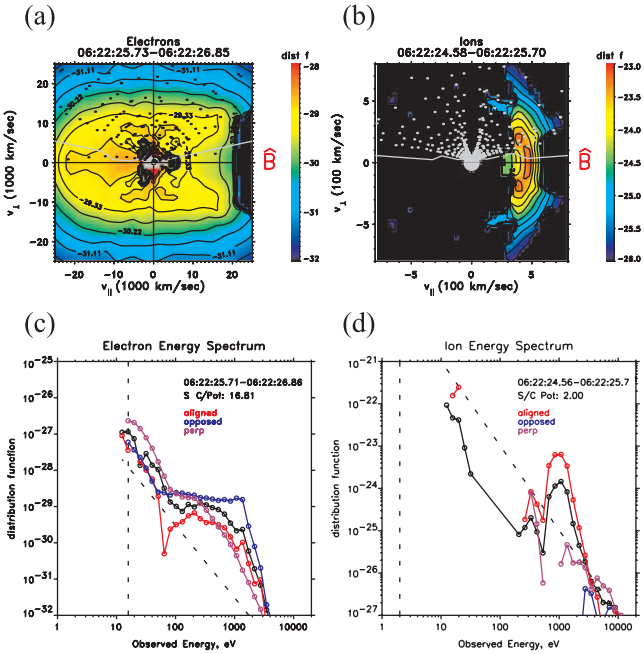

Figure 3. Electron (a) and ion (b) distribution functions in $v_{\|} - v_{\perp}$ space in the vicinity of the $E_{\|}$ event at 0622:26. Also shown are the corresponding electron (c) and ion (d) energy spectra aligned (red curve), opposed (blue curve), and perpendicular (magenta curve) to the magnetic field vector. The omnidirectional spectrum is indicated by the black curve.

0622:30 UT associated with the downward electron enhancements seen in Figure 2j indicates predominantly downward electron fluxes.

[13] One-second resolution electron and ion velocity space distribution functions near 0622:26 are illustrated in Figures 3a and 3b, respectively. In the southern auroral zone positive (negative) values of $v_{\|}$ are associated with particles moving away from (toward) Earth. Corresponding one-second resolution cuts of the electron and ion distribution function aligned (red curve), opposed (blue curve), and perpendicular (magenta curve) to the magnetic field vector $\hat{\mathbf{b}}$ are exhibited in Figures 3c and 3d, respectively. The solid black curve represents the energy spectrum averaged over all pitch angles. The spectra depicted in Figures 3c and 3d have not been corrected for the spacecraft floating potential. The dotted vertical line indicates the spacecraft potential. The dotted diagonal line represents the average one-count level of the 1.15-s sampling interval. The spectra are averaged over a finite pitch angle extent of roughly 30°. Some of the bins used to get the average spectra have no counts, thus at times the spectra may fall below the average one-count level. The downward cut (blue curve) of the electron distribution function in Figure 3c is basically flat with a phase space density that is an order of magnitude larger than the upward cut (red curve). This is characteristic of a modified loss cone distribution of electrons which results from the interaction of magnetized electrons with the parallel potential and mirroring magnetic field. In going from the plasma sheet to the ionosphere, a fraction of the electrons get mirrored. However, a parallel electric field exists and accelerates enough electrons through the magnetic mirror, so as to guarantee quasineutrality and maintain current balance. The flat part of the distribution function is often interpreted as the end state of an accelerated electron beam after quasi-linear plateau formation.

[14] The vertical extent of the potential that results from the parallel electric field signature can be obtained by assuming that the large-amplitude parallel electric field is constant and is responsible for all of the potential drop experienced by the electrons (ions) in going from the magnetosphere (ionosphere) to the spacecraft. The first approximation is a very crude approximation of the functional form of the parallel field and is equivalent to assuming a linear potential ramp in the magnetosphere-ionosphere transition region. The latter assumption is motivated by the recent simulations by *Ergun et al.* [2000], who suggested the existence of significant parallel potential drops concentrated in very thin layers ($\lesssim$125 km). Both assumptions yield a reasonable order of magnitude estimate of the vertical extent of the potential due to the large parallel electric field signature. The high-energy limit of the plateau in the parallel electron distribution profile given in Figure 4c provides a rough measure of the potential above the spacecraft seen by the electrons. Using the observed values of 35 mV/m and 1 keV for the parallel electric field amplitude

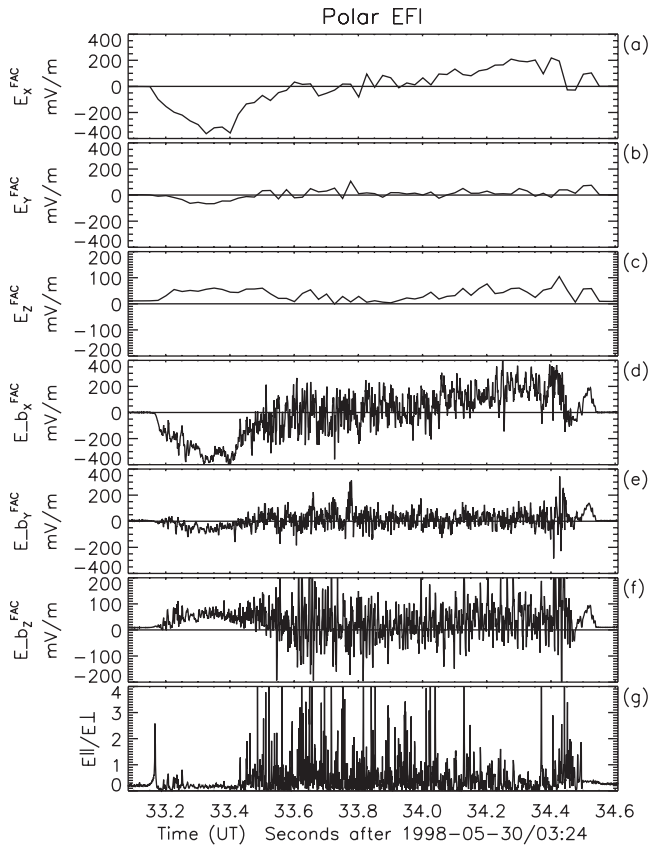

Figure 4. A southern auroral zone crossing near local midnight on 30 May 1998. Shown are (a)–(c) the components of the electric field vector in field-aligned coordinates sampled at 40 Hz, (d)–(f) the components of the electric field vector in field-aligned coordinates sampled at 1600 Hz, and (g) the ratio $E_{\|}/E_{\perp}$.

and the parallel potential, the vertical extent of the potential above the spacecraft is estimated to be ≈30 km. The ion distribution is a beam, which suggests a net parallel potential of ~1 keV and hence an estimated 30 km vertical extent below the spacecraft.

[15] Our estimates of the altitudinal extent of the parallel potential suggest that if all or most of the parallel potential drop seen by the particles is due to the large-amplitude parallel electric field, then the auroral acceleration region must be confined to a narrow region roughly tens of kilometers in extent, as opposed to thousands of kilometers. However, previous observations [*Mozer and Hull*, 2001] suggest via observations of inverted-V electrons at higher altitudes ($2R_E$ to $5R_E$) the existence of weak parallel electric fields. Thus it is likely that these large-amplitude parallel electric fields observed at low altitudes are accompanied by weaker parallel electric fields at higher altitudes. What is not obvious is whether most of the parallel potential drop seen by the particles is due to the large-amplitude parallel electric field at low-altitudes, the weak parallel electric fields at higher altitudes, or if significant contributions come from both. Accordingly, our estimates represent an upper limit on the vertical extent of the parallel potential drop associated with the large-amplitude parallel electric fields. In other words, if there are significant contributions to the total potential drop experienced by the electrons from weak parallel fields at higher altitudes, then the potential drop due to the strong parallel electric field at lower altitudes will be confined to a thinner region than implied by our calculation.

[16] The presence of both upward accelerated ions and downward precipitating electrons suggests that Polar is traversing the upward current portion of the auroral acceleration proper. A model of the equipotential configuration along the field line consistent with the observations is given in Figure 1c. The auroral zone proper is envisaged to be composed of a pair of U-shaped, elongated structures with intense parallel electric fields occurring in a highly localized region (tens of kilometers) near the bottom of the potential tongues, and weak parallel electric fields at higher altitudes. This scenario is to be contrasted with the generally accepted paradigm of the equipotential morphology, which is viewed to be U-shaped, with a parallel potential distributed over thousands of kilometers as depicted in Figure 1a. The inferred orientation of the electric potential structure encountered by Polar can be estimated by the angle $\alpha = \tan^{-1}(E_\perp/E_\parallel)$. The large $E_\parallel E_\perp$ ratios of 15 and 10 that characterize the $E_\parallel$ events suggest boundary crossings with respective normals inclined at angles of 4° and 6° with respect to magnetic field. Thus, we view Polar to be traversing the bottom edge of the potential tongues within the region of concentrated parallel potential due to a large-amplitude parallel electric field, as indicated by the dashed arrow in Figure 1c.

3.2. 30 May 1998 Event

[17] Macroscopic parallel electric fields with significant amplitude were observed by Polar on 30 May 1998, at an altitude of about 5400 km. Polar was near midnight at an invariant magnetic latitude of ~67°, and was moving poleward. The K_p index for these events was 4. The region is characterized by an upward field aligned current with an amplitude of roughly 0.3 $\mu A/m^2$ estimated from the slope (gradient) of the magnetic field perturbation (data not shown). Figures 4a–4c depict time series of the 40-Hz sampled electric field data in the FAC system. Large scale $E_\parallel$ occur in two intervals (0324:33.2–0324:33.7 UT and 0324:34.0–0324:34.8 UT, respectively) with peak amplitudes ranging from 65 to roughly 100 mV/m (see Figure 4c). The $E_\parallel$ structures are nearly coincident with large-amplitude $E_\perp$ structures shown in Figure 4a and have a sense such that $\mathbf{J} \cdot \mathbf{E} > 0$. The peak $E_\parallel/E_\perp$ ratios were found to be 0.25 and 0.5, respectively, suggesting asymmetric in-out boundary crossings with inward pointing normals inclined 75° and 63° with respect to the magnetic field vector. The large-amplitude parallel electric fields encountered in this event cannot result from errors in the magnetic field direction. There would have to be errors of 15° and 27°, respectively, whereas the uncertainty in the magnetic field direction is known to be within a few degrees. The transverse extent of these structures is estimated to be 3.5 and 5.6 km, respectively, assuming a static model (see discussion below on the validity of the static assumption), which is of the order of the electron inertial length, $c/\omega_{pe} \approx 3$ km. Hydra was unable to measure the electron and ion distribution function over the short time span the parallel electric field structures took to convect by the spacecraft.

[18] The 40-Hz electric field observations do not preclude the possibility that the $E_\parallel$ signatures were caused by higher frequency oscillations. For example, the $E_\parallel$ structures could represent the envelope of a more or less unipolar, higher frequency wave packet, as observed in the plasma sheet boundary [e.g., *Cattell et al.*, 1998b]. In addition, the rectification of waves with angular frequencies above the inverse plasma sheath-sphere RC time could induce DC offsets in the probe potential measurements [*Boehm et al.*, 1994], which could show up, in the transformed data, as a parallel electric field structure. This rectification effect is due to the nonlinear response of the detector to the higher frequency wave. To show that these two different effects are not causing the $E_\parallel$ signatures, Figures 4d–4f display the components of the electric field constructed from data sampled at 1600 Hz through a 500-Hz low-pass filter. In addition to the long duration, large-amplitude structures seen in the 40 Hz data, the burst data reveals the presence of short duration solitary-like structures of significant amplitude (200–300 mV/m), occurring in the interval from 0324:33.5UT to 0324:34.4 UT. The impulsive structures have significant power, both parallel and perpendicular to the magnetic field vector. Figure 4g shows a times series of the $E_\parallel/E_\perp$ ratio that characterizes the entire interval. The interval over which the spiky structures occur only partially overlaps regions containing macroscopic $E_\parallel$ structures, which suggests that the macroscopic $E_\parallel$ structures are not the envelopes of unipolar, higher frequency wave packets, and are not caused by rectification effects.

[19] To distinguish the nature of the larger scale parallel electric field events from the spiky structures, it is useful to perform a wavelet analysis. Figures 5a–5c display the time-frequency power spectra of the electric fields given in Figures 4d–4f, respectively. The power spectra were based on a Morlet wavelet [e.g., *Torrence and Compo*, 1998], which is ideal for resolving localized structures. The dotted

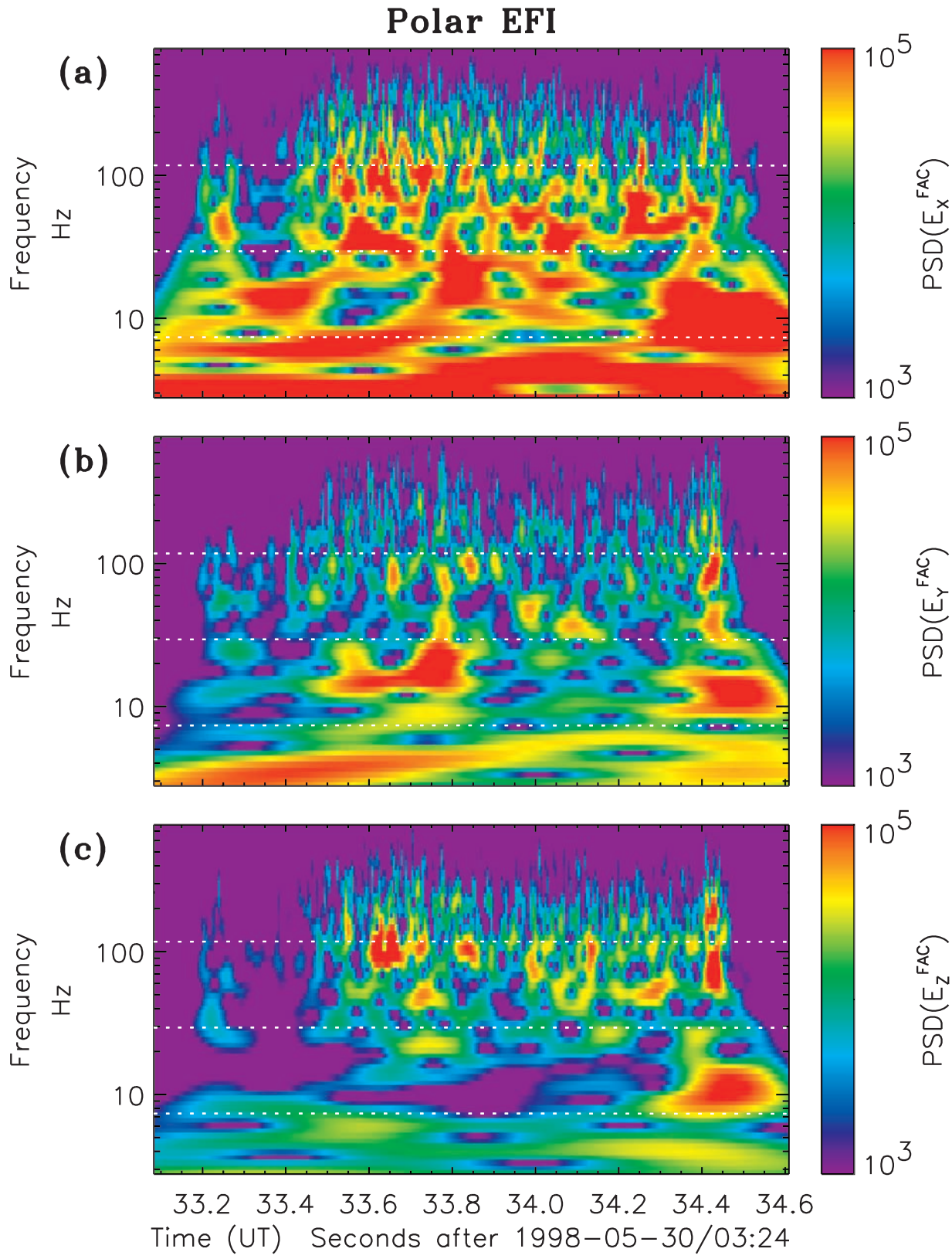

Figure 5. Time-frequency power spectra based on Morlet wavelet analysis of the three components of the burst electric field vector in field-aligned coordinates.

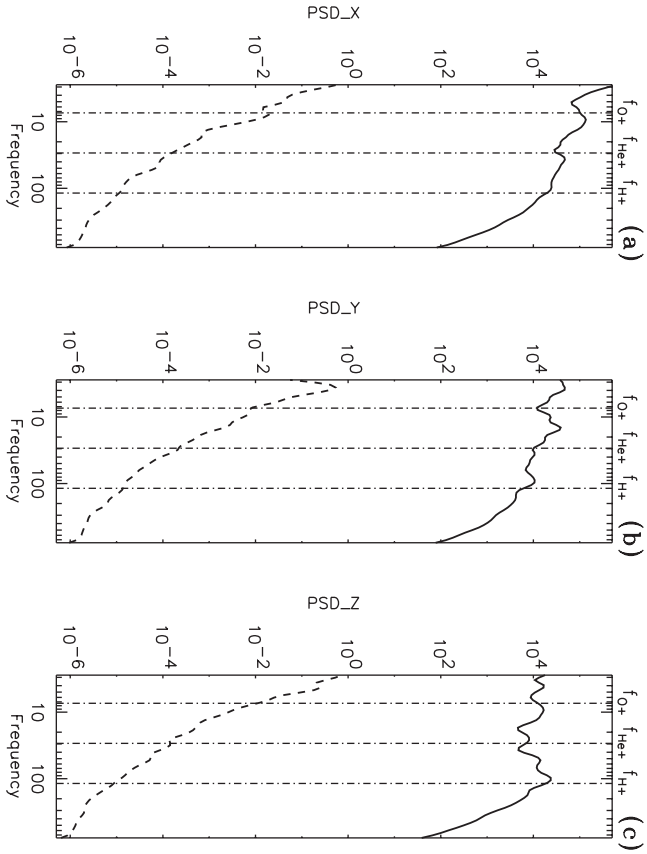

Figure 6. The power spectra of the components of the burst electric field data in the FAC system (solid curve) and corresponding search coil magnetic field power spectra (dashed curves).

white lines at 120, 30, and 7.4 Hz in Figures 5a–5c represent the H^+, He^+, and O^+ gyrofrequencies, respectively. The macroscopic structures are manifested in the frequency regime $\lesssim$10 Hz, whereas the spiky structures have peak power at frequencies near f_{H^+} and f_{He^+}. The transverse electric field has considerable broadband power in the north-south direction (see Figure 5a), with substantially less power in the east-west direction (see Figure 5b). A sharp separation of scales is apparent in the parallel component depicted in Figure 5c. Namely, the power is substantially depressed at frequencies slightly above 10 Hz, which does not occur in the perpendicular components.

[20] The spectral density of the electric field (in units of $(mV/m)^2/Hz$) averaged over the interval from 0324:33.1 UT to 0324:34.6 UT are indicated by the solid curves in Figures 6a–6c. The vertical lines in Figures 6a–6c indicate the gyrofrequencies f_{H^+}, f_{He^+}, and f_{O^+}. The AC magnetic field search coil data are available for this event, however, we saw no significant perturbations, with the search coil signal being indistinguishable from the background magnetic field noise observed in neighboring quiet regions. For completeness, the power spectra (dashed curves) of the search coil magnetic fields (in units of $(nT)^2/Hz$) have been included in Figures 6a–6c. The lack of any noticable magnetic field perturbation associated with the electric field data suggests that the electric fields are electrostatic in character.

[21] The electrostatic character and the near coincidence of the spectral peaks with the characteristic gyrofrequencies in Figures 6a–6c suggest that the spiky structures are H^+ and He^+ ion cyclotron waves, which have been commonly observed in the auroral acceleration region [e.g., *Mozer et al.*, 1977; *Kintner et al.*, 1979; *Cattell et al.*, 1991, 1998a]. The fact that the broad $E_\parallel$ structures partially overlap the oxygen gyrofrequency regime may lead one to believe that the macroscopic parallel electric field structures due to oxygen cyclotron fluctuations. However, we performed a time-of-flight analysis using potential measurements from opposing probes and found that the large scale structures are static structures convecting by the spacecraft at the spacecraft speed. The validity of an oxygen cyclotron description would require the wave vector to have a preferred alignment relative to the spacecraft trajectory, a scenario which is possible, but unlikely. Moreover, the large scale $E_\parallel$ structures are not oscillatory in nature, but appear, in this example, nearly coincident with a pair of macroscopic, converging $E_\perp$ structures often called electrostatic shocks.

[22] Alfvén waves can have a significant parallel electric field component and can appear to be electrostatic, especially for structures that are sufficiently narrow in the direction transverse to the magnetic field [e.g., *Lysak and Lotko*, 1996; *Lysak*, 1998; *Stasiewicz et al.*, 2000, and references therein]. We explored the possibility that kinetic Alfvén waves are responsible for the large-amplitude, macroscopic parallel electric field signatures by establishing whether the ratio $v = V_A B_Y / E_X$ associated with the field signatures of interest is consistent with the predictions of the kinetic Alfvén wave model given by *Lysak* [1998]. Over the frequency regime ($\lesssim$10 Hz) corresponding to the macroscopic parallel electric field signatures, the ratio $v_{obs} = V_A B_Y / E_X$ was found to vary from 5×10^{-3} to 5×10^{-2}. The kinetic Alfvén wave expectation for the ratio v_A is plotted as a function of V_e/V_A and $k_\perp c/\omega_{pe}$ in Figure 1 of the paper by *Lysak* [1998]. In this event the electron temperature varied from 0.5 to 1 keV and the density varied from roughly 0.5 to 10 cm^{-3} in the vicinity of the parallel field signatures. The perpendicular widths of the field structures were determined previously. Using these values we determined that $k_\perp c/\omega_{pe} \approx 2\pi c/(\omega_{pe} L_\perp)$ ranges from 3.0 to 10 and V_e/V_A ranges from 0.3 to 0.4. These values suggest an Alfvén wave expectation for the ratio $v_A \sim 0.4$ to 0.9, which is one to two orders of magnitude larger than v_{obs}. Thus, we conclude that the kinetic Alfvén wave explanation for the occurrence of the macroscopic parallel electric field structures is not plausible in this case.

3.3. 20 July 1997 Event

[23] Figure 7 illustrates another example of large-amplitude parallel electric fields. The three hour averaged K_p was 2. Large $E_\parallel$ events were observed at ~1308:15 UT with peak amplitudes of 84 and 76 mV/m, respectively. The events are coincident with $E_\perp$ structures with respective amplitudes of 190 and 140 mV/m. We emphasize that these parallel electric field signatures are not the result of the projection of a purely perpendicular field due to errors in the magnetic field direction. The estimated uncertainty in the direction of the magnetic field is within a few degrees. Unreasonably large angular uncertainties of 24°

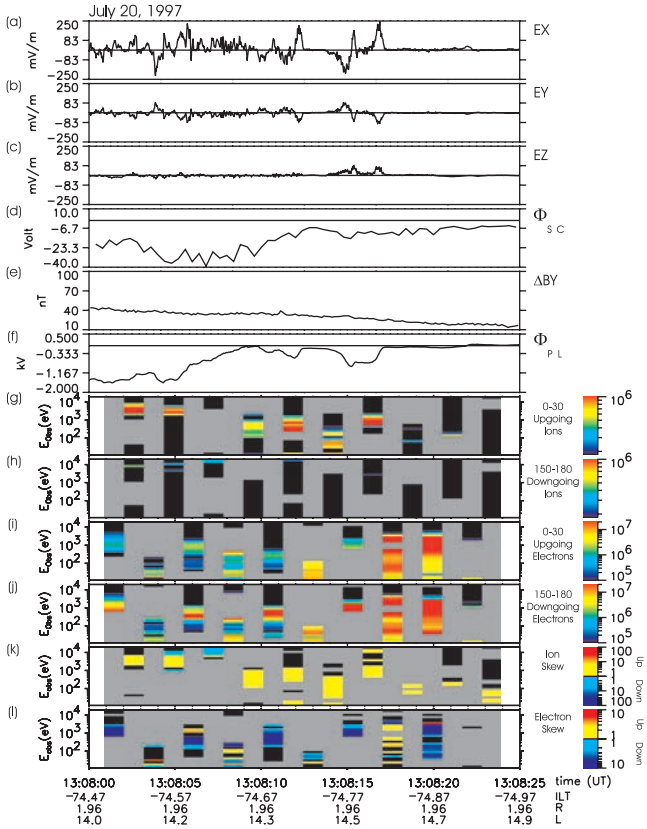

Figure 7. A southern auroral zone crossing in the evening sector on 20 July 1997. Shown are (a)–(c) the components of the electric field vector in field-aligned coordinates, (d) the spacecraft potential, (e) the east-west perturbation magnetic field, (f) the plasma potential, (g)–(h) spectrograms of field-aligned and field-opposed differential ion energy flux, respectively, (i)–(j) spectrograms of field-aligned and field-opposed differential electron energy flux, and spectrograms of the (k) ion skew and (l) electron skew.

and 28°, respectively in the magnetic field direction would be required for the parallel electric fields to be explained by this effect. The region was characterized by an upward field-aligned current with an amplitude of 0.14 $\mu A/m^2$ (slope of ΔB_Y illustrated in Figure 7e). The $E_{\|}$ events occurred in moderately depressed density regions of $\sim$1 cm^{-3} compared to the peak quiet region density of about $\sim$50 cm^{-3} as is inferred from the Φ_{SC} given in Figure 7d. The events are relatively narrow, characterized by spatial widths transverse to the magnetic field of 9 km (0.9 c/ω_{pe}) and 5 km (0.6 c/ω_{pe}), respectively. These events are particularly interesting because particle measurements were acquired during times concurrent with the large parallel field. Upward moving ions (see Figures 7g and 7h), and downgoing electrons (Figures 7i and 7j) are shown to be coincident with the $E_{\|}$ structures. The parameter Φ_{pl} given in Figure 7f suggests a $\sim$1 keV potential drop below the S/C.

[24] Cuts of the electron and ion distribution function aligned (red curve), opposed (blue curve), and perpendicular (magenta curve) to the magnetic field vector are exhibited in Figures 8a and 8b, respectively. The black curve denotes the omnidirectional energy spectrum. The downward cut (blue curve) of the electron distribution function in Figure 8a is sharply peaked at 1 keV with a phase space density that is more than an order of magnitude larger than both the field-aligned (red curve) and perpendicular (magenta curve) cuts. Similarly, the upward cut (red curve) of the ion distribution is sharply peaked at 500–600 eV, with little or no phase space density in the downward

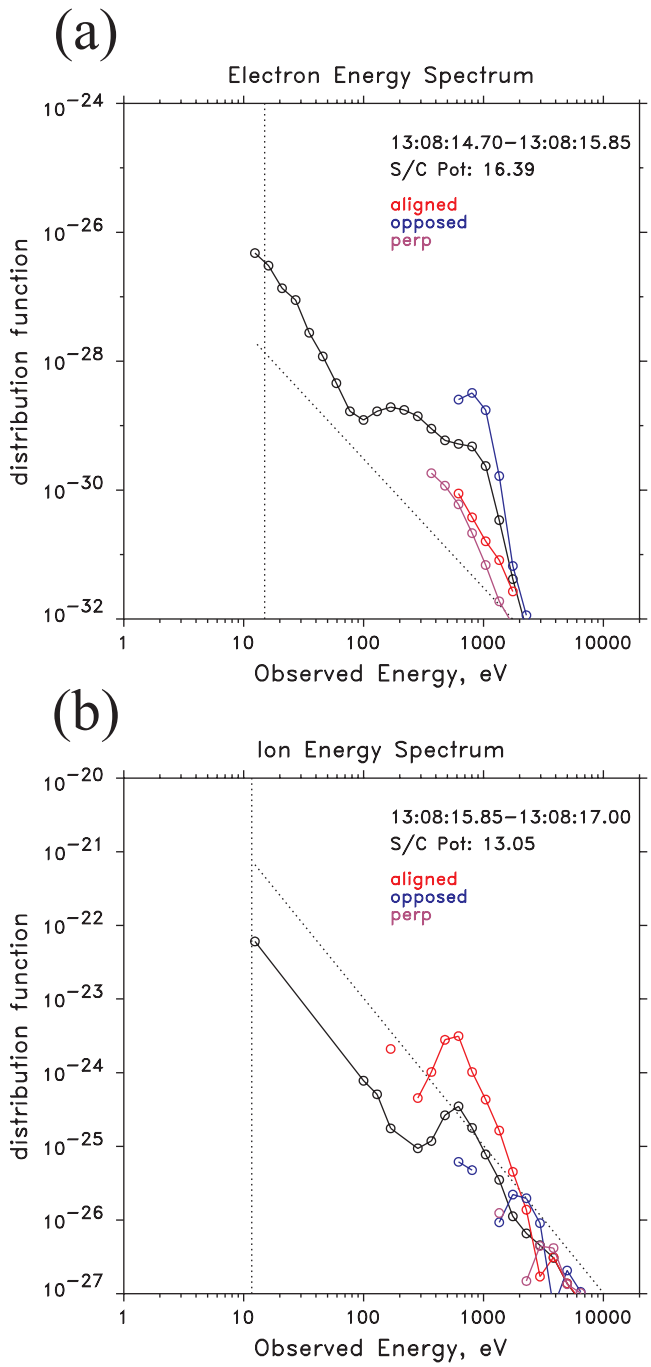

Figure 8. The (a) electron and (b) ion spectra in the vicinity of the $E_{\|}$ events. The color code denotes the spectra aligned (red curve), opposed (blue curve), and perpendicular (magenta curve) to the magnetic field vector. The black curve denotes the omnidirectional energy spectrum.

and perpendicular cuts. The energy of the ion beam is consistent with the Φ_{pl} expectation for the potential below the spacecraft. Estimates of the vertical extent of the parallel potential are roughly 10 km above and 5 km below the spacecraft, assuming a constant parallel electric field that is responsible for all of the electron and ion acceleration.

3.4. 4 April 1996 Event

[25] As an illustration of one of the largest $E_{\|}$ amplitudes encountered by Polar, Figure 9 depicts field and particle data for a southern crossing near local midnight on 4 April 1996, featured in an earlier study [*Mozer and Kletzing*, 1998]. The region is characterized by a K_p index of 2 and a uniform upward field-aligned current with an amplitude of 0.01 $\mu A/m^2$ (see Figure 9e). Polar enters a region of depleted density at ~2044:27 UT (see Figure 9d). The high to low density ratio is roughly 50. The perpendicular component of the electric field (see Figures 9a and 9b) is of small amplitude (~50 to 100 mV/m at the edges of the density cavity, and reaching much smaller values within the density cavity). The parallel electric field component is nearly zero, except at ~2044:46 UT, where the amplitude reaches 250 mV/m (Figure 9c). The $E_{\|}/E_{\perp}$ ratio corresponding to the large parallel field signature is roughly 8. The plasma density associated with the large $E_{\|}$ signature is about 0.07 cm^{-3}, which is an order of magnitude less than the 0.5 cm^{-3} peak density in the interval immediately following the $E_{\|}$ signature. The perpendicular width of the parallel field is estimated at 0.9 km (~0.1 c/ω_{pe}), which maps down to roughly 300 m at ionospheric altitudes.

[26] Within the density cavity region (~2044:27–2044:45 UT), upgoing ion beams are observed (see Figures 9g and 9h). It is important to note that the upgoing ion beams are quite narrow in pitch angle and Hydra, with gaps in its angular sampling, captures the narrow beam occasionally through the interval, and only when one of the pairs of detectors is nearly aligned (within 30°) along the magnetic field line. This was the case for the samples taken at 2044:29, 2044:35, 2044:45, and 2044:47 UT. In all of the other ion sampling intervals, the angle between the nearest detector look direction and the magnetic field direction was greater than 30°, and thus ion beams along the magnetic field direction (if present) were not seen by Hydra.

[27] In contrast, the full electron distribution is well measured by the Hydra detector. Figures 9i and 9j show that downgoing electrons are present inside the density cavity. The dropouts in the upgoing electron differential energy flux between 2044:24 and 2044:45 UT signify the existence of a parallel potential below the spacecraft, which prevents electrons of ionospheric origin from accessing this altitude. The electron and ion signatures coupled with the electric field observations inside the density cavity suggest that Polar is within an acceleration region characterized by a parallel potential that is distributed over a large spatial extent (thousands of kilometers). The Hydra detectors were unable to measure the particle properties over the short time interval over which the large-amplitude parallel electric field structure occurred, though upgoing ions and downgoing electrons were observed in the vicinity of the $E_{\|}$ event with peak beam energies of about 0.5 kV. This suggests a parallel potential that is distributed over a few kilometers.

[28] Figure 1d displays one possible model of the potential distribution that can explain these observations. Within the density cavity, the equipotential contours are envisioned to be distributed over a large spatial extent, whereas at the outgoing edge of the density cavity the potential contours are kinked or S-shaped. This event illustrates the complex nature of the auroral acceleration region, namely, the potential can be distributed over a large spatial extent and also be sheath-like in structure within a given current region. As to what determines whether the potential is highly localized in space or not is still not well understood. A detailed analysis suggests that ambipolar effects may be important (see discussion below in section 5).

3.5. 13 October 1996 Event

[29] In contrast with the nonoscillatory, macroscopic $E_{\|}$ structures discussed in sections 3.1–3.4, we provide, in this section, an example with large parallel and perpendicular oscillations which appear to be those of oxygen cyclotron waves. The occurrence of electric field oscillations at frequencies below the 40 Hz sampling which have a significant parallel component was rare at the altitudes sampled by Polar in the southern auroral zone. The event occurred near local midnight on 13 October 1996 at an altitude of ~6000 km. The K_p index was 2-, suggesting relatively quiet global auroral activity. Figure 10 summarizes the particle and field data for this event. This example contains parallel electric field fluctuations (Figure 10c) with peak amplitudes ranging from 50 to 200 mV/m. In this event the density makes a transition from ~20 cm^{-3} to roughly 10^{-3} cm^{-3} as inferred from Φ_{SC} given in Figure 10d. The slope of ΔB_Y (Figure 10e) suggests that the $E_{\|}$ fluctuations occur in a region of upward field aligned current. The $E_{\|}$ amplitude is oscillatory in nature, and becomes most pronounced from 1318:31 to 1318:33 UT, which corresponds to the region of lowest density (or largest negative Φ_{SC} illustrated in Figure 10d). Intense field-aligned ion beams with mean energy of ~1 keV are shown to be concurrent with the low density region. The amplitude and energy of the ion beams is consistent with Φ_{pl}. At this time resolution, the electrons were not well sampled along **B** in the density cavity, although the distribution function in $v_{\|}-v_{\perp}$ space (not shown) is consistent with precipitating electrons.

[30] To better establish the properties of the fluctuations, we separated the higher frequency components from the macroscopic structure by boxcar averaging the electric field components depicted in Figures 10a–10c using a sliding boxcar window of six points (0.4 sec resolution) and then subtracting this result from the unaveraged field components. The resulting detrended AC components of the electric field are given in Figures 11a–11c. The corresponding macroscopic fields are depicted in Figures 11d–11f. The spacecraft potential profile is provided in Figure 11g, as a reference. The parallel fluctuations are coincident with perpendicular fluctuations of similar amplitude. Throughout most of the interval, parallel spikes depicted in Figure 11c are accompanied by spikes in either one or both of the perpendicular fields depicted in Figures 11a and 11b. The correlation coefficient between the magnitudes of the parallel and perpendicular AC electric fields was 0.5. This strong correspondence suggests that the perpendicular and parallel fluctuations are from the

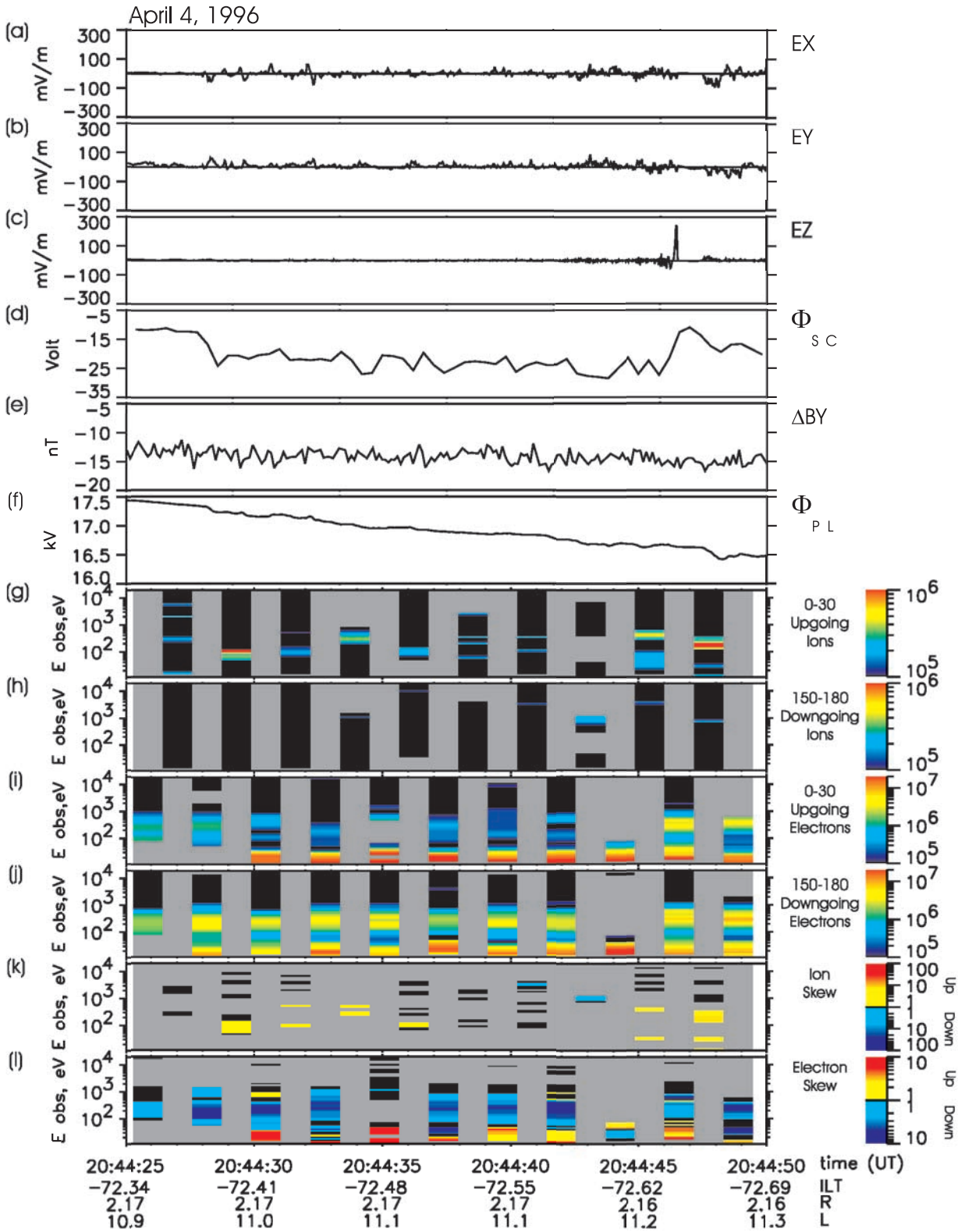

Figure 9. A southern auroral zone crossing near local midnight on 4 April 1996. Shown are (a)–(c) the components of the electric field vector in field-aligned coordinates, (d) the spacecraft potential, (e) the east-west perturbation magnetic field, (f) the plasma potential, (g)–(h) spectrograms of field-aligned and field-opposed differential ion energy flux, respectively, (i)–(j) spectrograms of field-aligned and field-opposed differential electron energy flux, and spectrograms of the (k) ion skew and (l) electron skew.

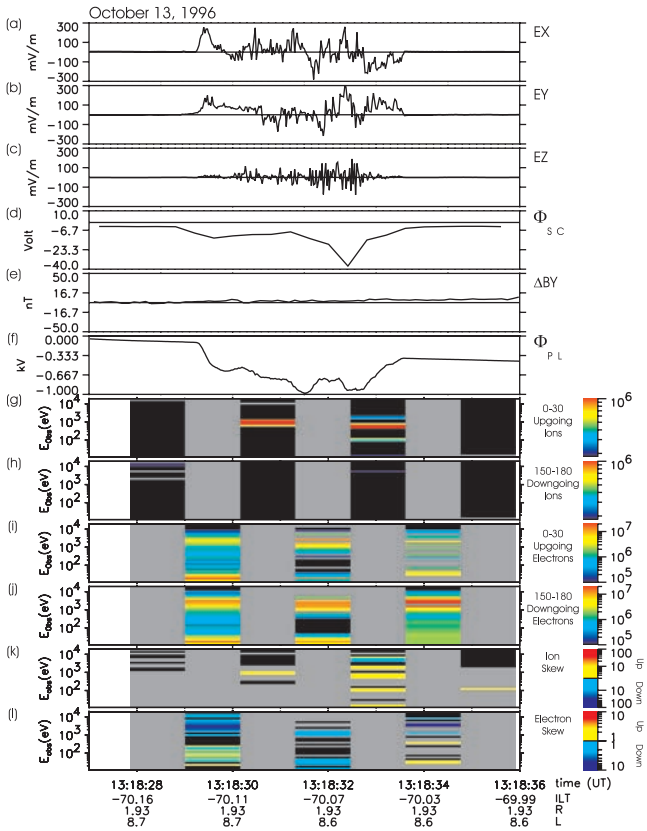

Figure 10. A southern auroral zone crossing near local midnight on 13 October 1996. Shown are (a)–(c) the components of the electric field vector in field-aligned coordinates, (d) the spacecraft potential, (e) the east-west perturbation magnetic field, (f) the plasma potential, (g)–(h) spectrograms of field-aligned and field-opposed differential ion energy flux, respectively, (i)–(j) spectrograms of field-aligned and field-opposed differential electron energy flux, and spectrograms of the (k) ion skew and (l) electron

same mode. In addition to the large $E_{||}$ fluctuations, there exists large-amplitude, macroscopic parallel electric fields which range in amplitude from 40 to 70 mV/m occurring at ~1318:30 UT and ~1318:32, respectively (see Figure 11f). The respective $E_{||}/E_{\perp}$ ratios are found to be 0.6 and 1.0. The macroscopic events are characterized by a transverse width of roughly 2 km. In stark contrast with the parallel field oscillations, the macroscopic fields are not oscillatory in nature, appearing as a unipolar signature of a sense to accelerate ions upwards and electrons downward. This unipolar feature is a recurring property of the $E_{||}$ events that make up this database.

[31] To provide insight into the identity of these fluctuations, Figures 12a–12c display the power spectra of the electric field components depicted in Figures 10a–10c, within the cavity. The solid curve in each of the figures represents the power spectra of the unaveraged electric field and the dotted curve represents the power spectra of the detrended AC electric field components. The peaks in all 3 components of the field near 3 Hz reflects the macroscopic structure. In addition, all three components show a significant peak at about 7–8 Hz, which is roughly at the oxygen gyrofrequency f_{O^+} indicated by the solid vertical line. The near coincidence suggests that these oscillations are consistent with oxygen cyclotron waves. The occurrence of oxygen cyclotron waves suggests the presence of O^+ with significant density. Moreover, the power spectra indicates that the parallel electric field component has significant power. Oxygen cyclotron waves with large parallel fields are expected to cause significant electron flux modulations, which ultimately produce flickering aurora. It is important to note that the peaks at the oxygen cyclotron frequency should be viewed with caution. Depending on the filter roll-off, significant power at up to twice the Nyquist frequency could contaminate the lower frequency components. Thus, it may be the case that the power at 7–8 Hz could be due to a combination of O^+ and He^+ cyclotron modes (which if present should occur at ~30 Hz). Additional peaks in the power spectra occur near the Nyquist frequency for both the FAC *Ex* and *Ez* components of the electric field. We do not have a reliable explanation for these peaks at this time.

4. Statistical Properties

[32] Polar provides nearly uniform invariant latitude (Λ) and magnetic local time (MLT) coverage of the southern auroral zone over the 3-year sampling period. In 3 years of EFI data, with a total of about 3000 inbound and outbound crossings of the auroral zone, roughly 60 events or 2% of the crossings contain large-amplitude parallel electric fields. This low observation rate is consistent with their typical vertical extents which are inferred to be, at most, a few tens of kilometers. In the following subsections, we compare the properties of the $E_{||}$ events with other parameters that characterize the auroral acceleration region.

4.1. Geographic Location of $E_{||}$ Samples

[33] Figure 13a shows the geographic location of the events that make up this database. The events trace out a pattern characteristic of the auroral zone location in Λ and MLT in Figure 13a. However, the events are clustered in the premidnight quadrant, with substantially fewer events near local noon. This tendency is qualitatively similar to the distribution of inverted-V electron events [*Lin and Hoffman*, 1979], ion beams [*Gorney et al.*, 1981], and electrostatic shocks associated with ion beams [*Bennett et al.*, 1983; *Redsun et al.*, 1985] observed in the auroral zone.

[34] Figure 13b shows a histogram of the altitudes at which the $E_{||}$ events were observed by Polar. The altitudes ranged from $0.8R_E$ to $1.5R_E$, which corresponds to 5000 to 9600 km. The limited altitude range over which the parallel electric fields occurred is artificial and reflects the altitudes sampled by Polar in the southern auroral zone over the first 3 years of its mission. Thus, large-amplitude parallel electric fields may exist at altitudes above and below those sampled in this study. Figure 13c gives the occurrence rate as a function of altitude, defined as $p(h) = \int p(h, \Lambda)\, d\lambda$, where $p(h, \Lambda)d\lambda = N_o(h, \Lambda)/N_s(h, \Lambda)$, $N_o(h, \Lambda)$ is the number of parallel field events encountered at a given altitude and invariant latitude satisfying our selection criteria and $N_s(h, \Lambda)$ is the corresponding number of times Polar encountered that same geographic location. The vertical bars centered in each altitude bin indicate the estimated errors based on Poisson statistics. The occur-

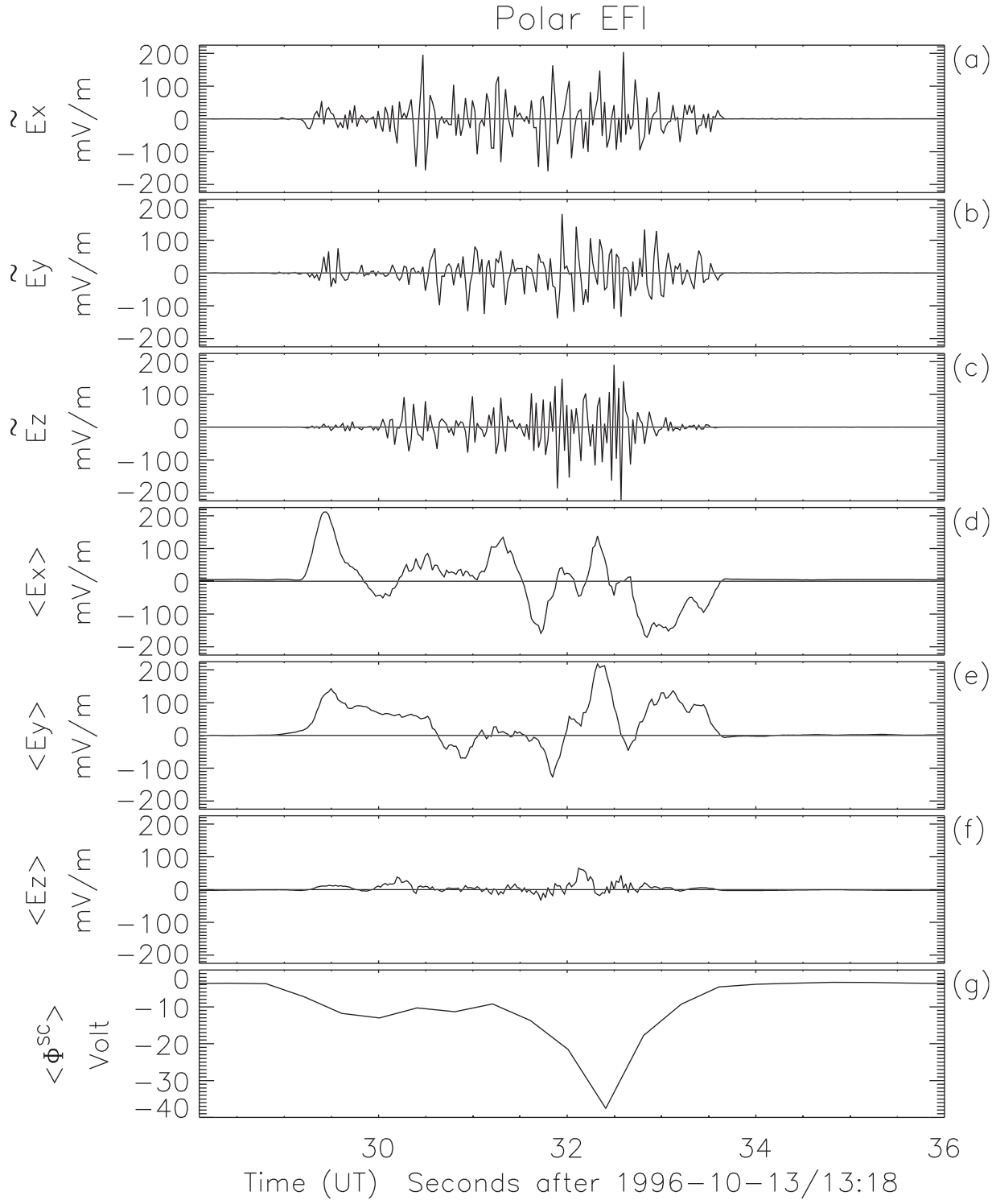

Figure 11. Depicts (a)–(c) the detrended AC components of the electric field, (d)–(f) the boxcar averaged electric field components, and (g) the spacecraft potential.

rence rate in Figure 13c peaks at an altitude of $\sim 1.28 R_E$, suggesting that the macroscopic parallel electric fields with amplitudes greater than our acceptance criteria of 25 mV/m tend to occur in a thin localized region. These results are consistent with the recent simulations by *Ergun et al.* [2000], which suggested the existence of thin layers containing significant potential drops and with the results of a recent survey [*Mozer and Hull*, 2001] of Polar data which found no evidence for large-amplitude parallel electric fields at much higher altitudes ($2-6 R_E$). Our results together with those of previous studies [*Mozer and Kletzing*, 1998; *Ergun et al.*, 2000; *Mozer and Hull*,

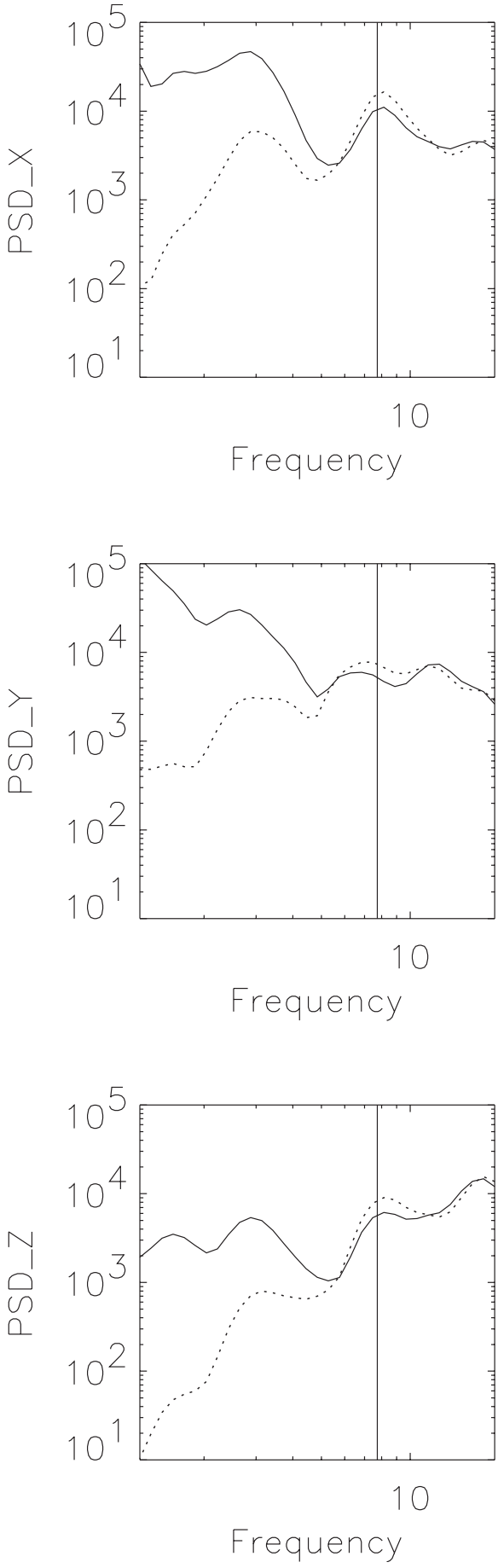

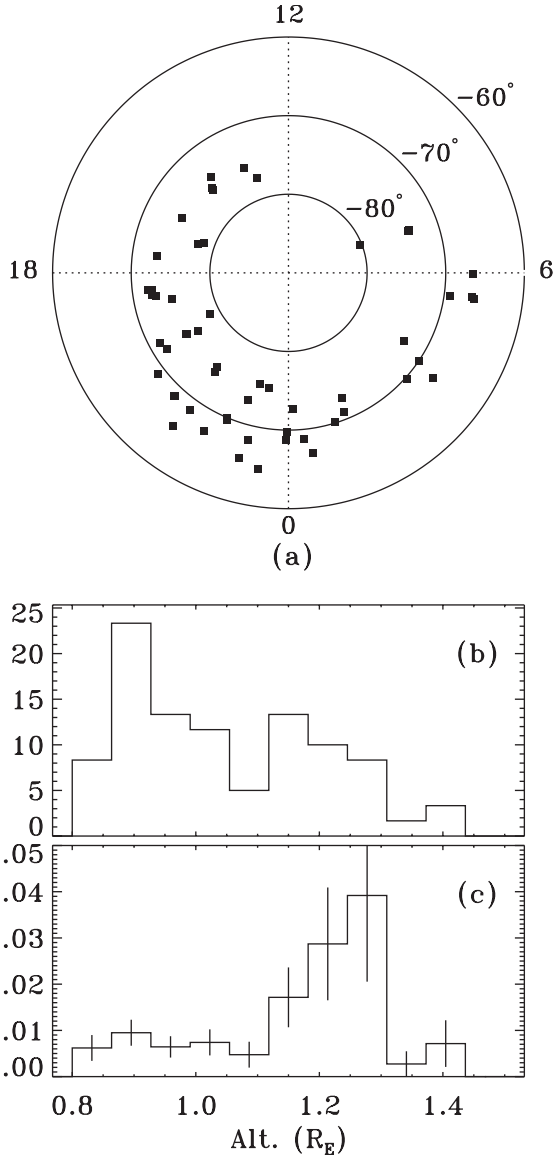

Figure 13. The geographic location of events as a function of invariant latitude and magnetic local time (a), a histogram of the sampled parallel electric field altitudes (b), and the occurrence rate as a function of altitude (c).

2001] suggest that the large-amplitude, macroscopic parallel electric fields are a property of the low-altitude portion of the auroral acceleration region.

4.2. Characteristic Amplitudes

[35] A summary of the characteristic electric field amplitudes of the events that make up this database is given in Figures 14a–14d. Figure 14a gives the distribution of the peak amplitude of the parallel electric events. The most probable peak value of the parallel electric

Figure 12. (opposite) The power spectra of the electric field data (solid curve). Also shown are the power spectra of the detrended AC electric field components (dotted curve). The solid vertical line indicates the oxygen gyrofrequency.

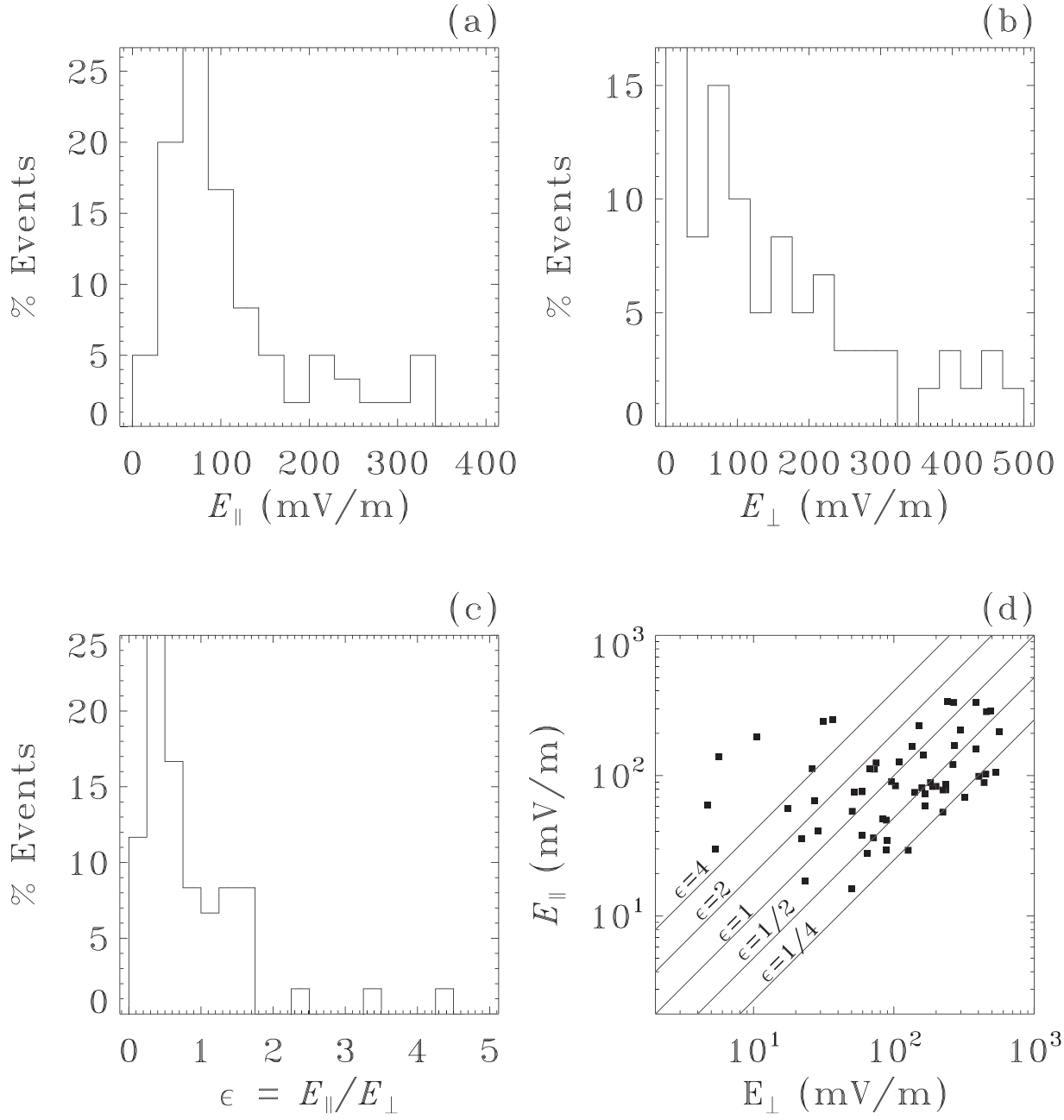

Figure 14. Histograms of (a) the magnitude of $E_\parallel$, (b) the magnitude of $E_\perp$, and (c) the ratio $\epsilon = E_\parallel/E_\perp$. Also shown (d) is a scatterplot of $E_\parallel$ and $E_\perp$. The solid lines represent different values of ϵ.

field, $E_{\parallel m}$, is found to be 70 mV/m, though much higher values are possible. The cutoff at low amplitudes is artificial and reflects the minimum amplitude of $E_\parallel$ selected for this study. Figure 14b is a histogram of the amplitude of the perpendicular electric field coincident with the peak parallel electric field of each event that makes up this study. Figure 14c is a histogram of the ratio $\epsilon = E_\parallel/E_\perp$ and Figure 14d is a scatterplot of $E_\parallel$ and $E_\perp$. The solid lines in Figure 14d represent different values of ϵ. The typical ϵ is 0.4 which indicates that large $E_\parallel$ events are concurrent with much larger $E_\perp$, although there are several events with much larger ratios. The ratio ϵ provides information on the geometries of the potential well encountered by Polar. Many of the events occur in the transition between high and low density plasma, with some events occurring within the acceleration proper. The typical orientation of the boundary normal characterizing the transition region is inclined at an angle $\alpha = \tan^{-1}(1/\epsilon) = 70°$. Values for $\epsilon \gtrsim 0.4$ are unlikely to be explained by uncertainties in the projection of a large, purely perpendicular field. Such a scenario would require errors of $\gtrsim 20°$ in the magnetic field direction.

[36] Figures 15a–15c shows the altitude dependence of the magnitudes of $E_\parallel$, $E_\perp$ and ε, respectively. There is no clear dependence between the magnitude of $E_\parallel$ and altitude, though there is a hint that the biggest $E_\parallel$ events are confined to lower altitudes. Figure 15c suggests that the largest $E_\parallel/E_\perp$

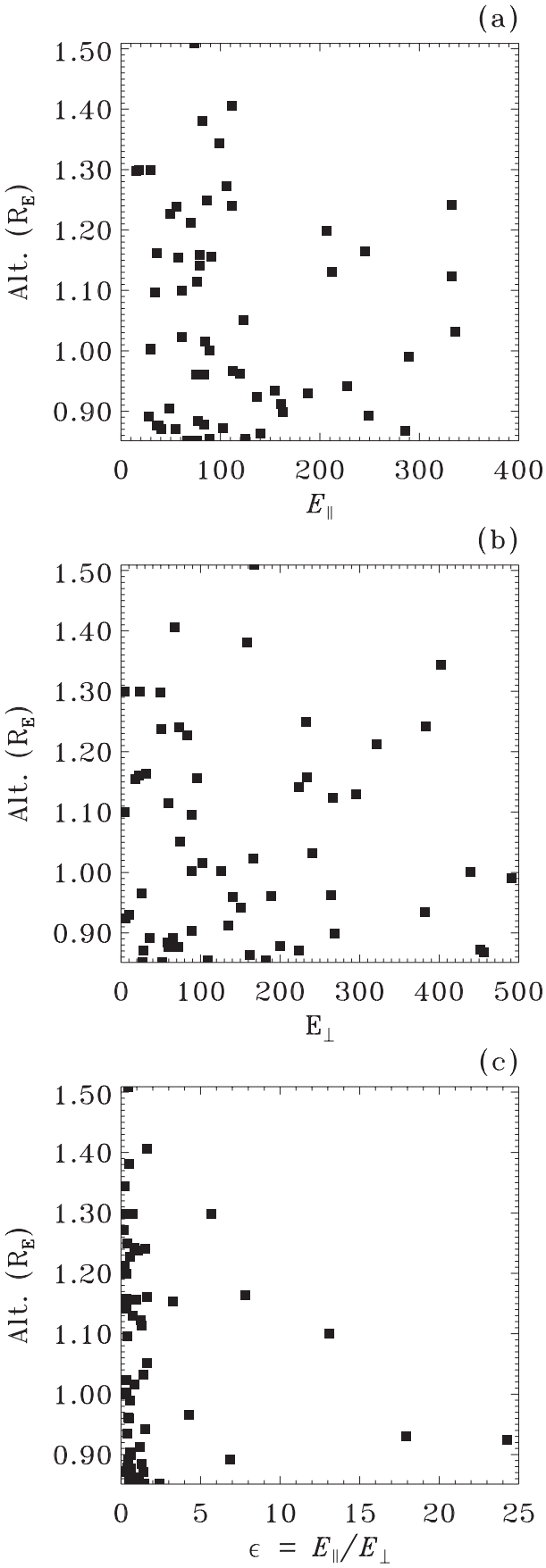

Figure 15. Observed altitude dependence of (a) $E_\parallel$ (b) $E_\perp$, and (c) $E_\parallel/E_\perp$.

ratios occur at the lower altitudes. This tendency is an indication of the geometrical sampling of the potential wells that make up this database and is consistent with the canonical electrostatic U-shaped model of the electron acceleration region, where the electric field is primarily perpendicular to the magnetic field at high altitudes and primarily field-aligned at low altitudes.

4.3. Comparisons With Parallel Current Density

[37] We explored whether or not the size of the parallel electric field is controlled by parallel current density. An appropriate measure of the current is the ratio $J_\parallel/B$ which for a given event should be a constant along a magnetic field line, provided the system is time stationary and the perpendicular current density is zero. The $J_\parallel$ was empirically inferred from $\nabla \times \Delta\mathbf{B}_{av} = \mu_0\mathbf{J}$, where $\Delta\mathbf{B}_{av}$ is the spin period averaged perturbation vector magnetic field and $\mathbf{J}$ is the current density. Linear interpolation was used to determine $J_\parallel$ at the time $E_\parallel$ occurred. Figures 16a–16c compare $J_\parallel/B$ with altitude, $E_\parallel$, and $E_\perp$Figure 16a indicates that there is no apparent altitude dependence on the current. The most probable value for $J_\parallel/B$ was found to be 2.0×10^{-11}A/(m^2 nT). There are events that have negative values, although a closer inspection of these events suggests that they may be explained by coarse sampling of $\Delta\mathbf{B}_{av}$ in a rapidly changing current region. Nevertheless, $\Delta\mathbf{B}_{av}$ provides a reliable estimate for $J_\parallel$ in an average sense. Figures 16b and 16c show no apparent $E_\parallel$ and $E_\perp$ dependence with current. However, there is a correlation between the direction of current and the direction of the parallel electric field, namely upward parallel electric fields are associated with upward pointing field-aligned current. Our search for parallel electric fields in this study was not restricted to the upward current part of the auroral region. The statistical preponderance of upward current associated upward directed field-aligned parallel electric fields adds credence to the measurements that make up our database. Moreover, the statistical correlation of the current sense with sense of the parallel electric field argues against an explanation of our results from random spurious electric fields; with such an explanation there should be no preference for the direction of current. It is important to note that the lack of any trend between upward parallel electric field amplitude and the current density does not invalidate the Knight relation which is a relationship between the parallel potential drop and the current density, although it does constrain it.

4.4. $E_\parallel$ Anticorrelation With Density

[38] Theoretical models of the auroral acceleration region [e.g., *Knight*, 1973; *Rönnmark*, 1999] predict, among other things, a relationship between the parallel electric field and the plasma density. Recent particle and field observations at higher altitudes [*Mozer and Hull*, 2001] also suggest the importance of the plasma density in determining the presence of parallel potential drops in the auroral zone. In particular, *Mozer and Hull* [2001] demonstrated that upgoing ions, which indicate significant parallel potential drops below the spacecraft, are not associated with variations in the current, but coincided with regions of depressed plasma density. Thus one might suspect that the large-

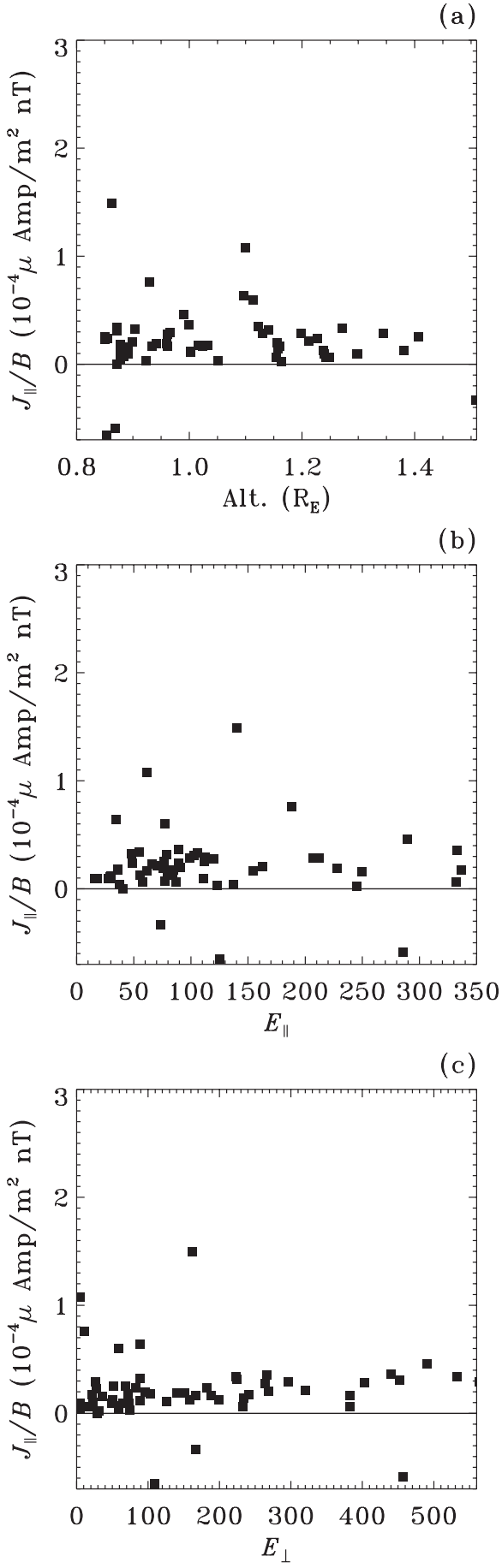

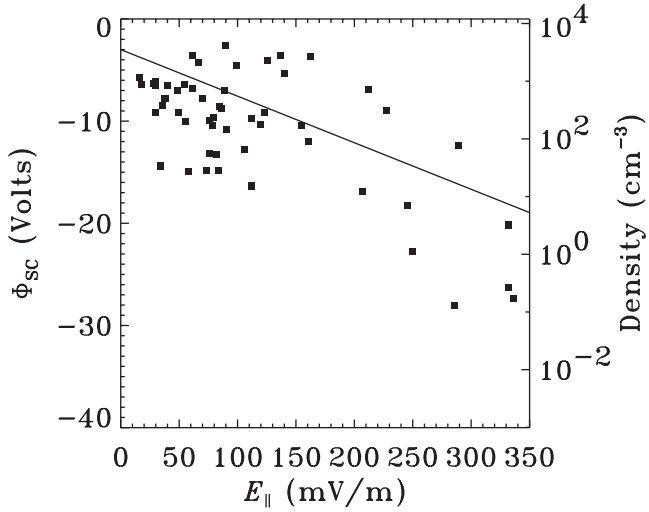

Figure 17. Comparison of the negative of the spacecraft floating potential Φ_{SC} with the measured parallel electric field $E_\parallel$.

amplitude parallel electric fields discussed in this paper should depend on the plasma density.

[39] Figure 17 compares $E_\parallel$ with Φ_{SC} or equivalently with the plasma density N. The density dependence depicted in Figure 17 was determined from the relation given by *Scudder et al.* [2000]. The comparisons in Figure 17 indicate that the amplitude of $E_\parallel$ increases with increasingly more negative values of Φ_{SC} or equivalently with smaller values of the plasma density. The best fit slope and intercept is found to be -0.05 km and -2.9 V, respectively, and the linear correlation coefficient is -0.69. The strong $E_\parallel$-Φ_{SC} anticorrelation illustrated in Figure 17 suggests a strong anticorrelation between $E_\parallel$ and the log(N). Although we did not directly measure the relationship between the plasma density and electric field along a given magnetic flux tube of force, our statistical result is suggestive of a such relationship in an average sense, given that the events sampled covers a broad altitude range. Such a dependence places a rather strict constraint on the mechanism or mechanisms responsible for supporting such large parallel electric fields. We interpret the anticorrelation to be a manifestation of an ambipolar response of the plasma at the interface between the low density magnetospheric plasma and the high density ionospheric plasma. The net result is a parallel electric field with a sense to accelerate electrons downward and ions upward to maintain current balance and quasineutrality (see discussion below in section 5 for more details).

4.5. Electric Field Transverse Widths

[40] In this section we summarize the properties of the transverse widths $W_{E\parallel}$ and $W_{E\perp}$ of the macroscopic parallel and perpendicular electric fields, respectively, that comprise this database. The $W_{E\parallel}$ is defined as the full width at half maximum of the $E_\parallel$ signature. Many of the $E_\parallel$ structures occurred nearly simultaneously with an $E_\perp$ structure which

Figure 16. (opposite) Comparisons of $J_\parallel/B$ (a) with altitude, (b) $E_\parallel$, and (c) $E_\perp$.

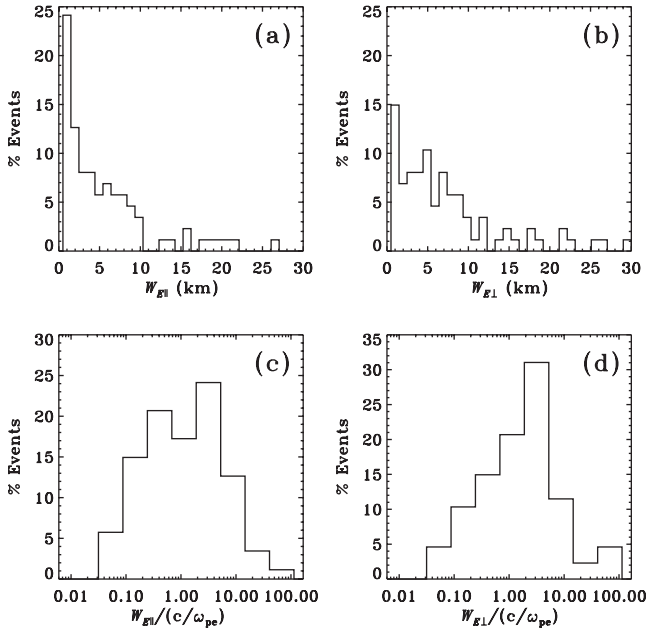

Figure 18. The distribution of the spatial widths of (a) the parallel electric field and (b) the corresponding perpendicular field structures. Also shown are the distributions of (c) $E_{\|}$ widths and (d) $E_{\perp}$ widths normalized by the electron inertial length c/ω_{pe}.

may be broader or narrower. However, a few cases (few percent) occurred in the center of converging pairs of $E_{\perp}$. Thus, we defined $W_{E\perp}$ as the full width at half maximum of the $E_{\perp}$ structure nearly coincident with a given $E_{\|}$ structure, or as the full width at half maximum of the nearest $E_{\perp}$ structure in those cases with $E_{\|}$ at the center of converging pairs of $E_{\perp}$. The macroscopic electric field structures were assumed to be convecting by the spacecraft at the orbital velocity in converting from temporal to spatial coordinates. Such an approximation was found to be valid for one of the examples discussed above via time-of-flight analyses of burst mode potential measurements from opposing sphere pairs (e.g., see the discussion in section 3.2).

[41] Histograms of $W_{E\|}$ and $W_{E\perp}$ are given in Figures 18a and 18b, respectively. The $W_{E\|}$ range in value from 0.5 to 26 km with a peak value at 1 km and median value of 4 km. The distribution of $W_{E\perp}$ is somewhat broader than the $W_{E\|}$ distribution, characterized by $W_{E\perp}$ ranging from 0.5 to 30 km, and peak and median $W_{E\perp}$ values of at 1 and 6 km, respectively. We imposed a lower spatial bound of 0.5 km in selecting the $E_{\|}$ events for this data set. The electric field estimates for events with spatial sizes much smaller than 0.5 km can be significantly impacted by finite wavelength effects in addition to possible density and temperature gradient effects. Thus, the lower cutoff value is artificial and smaller widths are possible, though we feel that they cannot be measured reliably by EFI.

[42] Earlier studies [e.g., *Mozer et al.*, 1980; *Mozer*, 1981] have investigated the spatial scales of auroral zone electric fields. In particular, the study by *Mozer et al.* [1980] suggested the presence of two spatial scale sizes for the perpendicular electric fields: (1) a broad scale of about a few degrees in invariant latitude (e.g., a few hundred kilometers at ionospheric altitudes) associated with the entire turbulent auroral zone electric field region, which may encompass several converging pairs of perpendicular fields, and (2) a much thinner scale $W'_{E\perp}$ ranging from 0.01° to 0.1° in invariant latitude (e.g., from 1 to 10 km at ionospheric altitudes) associated with a given pair of converging perpendicular electric fields. Our study focused on the spatial widths of a single electric field signature, as opposed to the spatial widths of a given pair of converging perpendicular electric fields. Thus, the perpendicular electric field transverse widths $W_{E\perp}$ presented in this study are roughly $W_{E\perp} \approx W'_{E\perp}/2$. The $W_{E\perp}$ in our study mapped to ionospheric altitudes corresponds to 0.17 to 10 km, which is roughly consistent with the 0.5 to 5 km range of widths inferred from the study by *Mozer et al.* [1980], although our estimates map to somewhat thinner structures at the ionosphere. The range of $W_{E\|}$ corresponds to roughly 0.17 to 8 km at ionospheric altitudes, with a distribution that is in rough correspondence with the distribution that characterizes the smallest scale sizes of discrete auroral arcs [e.g., *Maggs and Davis*, 1968]. Ultimately, the fine structure of auroral forms are connected with the detailed properties of the electron precipitation. Localized pockets of intense $E_{\|}$, such as those presented in this paper, could lead to fine scale enhancements of the energy flux of inverted-V precipitating electrons and hence to fine scale variations in discrete auroral arcs.

[43] Figures 18c and 18d depict distributions of $W_{E\|}$ and $W_{E\perp}$, respectively, normalized by the electron inertial length ($L_e = c/\omega_{pe}$). Estimation of ω_{pe} requires knowledge of the local plasma density, which was estimated from direct measurements of the spacecraft potential using the density-spacecraft voltage relation developed by *Scudder et al.* [2000]. Although somewhat broad, the normalized distributions given in Figures 18c and 18d show that the $W_{E\|}$ and $W_{E\perp}$ are typically the order of the electron inertial length. Other characteristic spatial lengths of interest are the electron Debye length λ_e and proton gyroradius r_p. At these altitudes, $c/\omega_{pe} \sim 20\ \lambda_e \sim 20 r_p$ (assuming 1 keV protons and an electron temperature $\sim$1 keV). Thus the typical widths of the fields are of the order of $20\lambda_e$ or $20r_p$.

4.6. Association With Global Auroral Activity

[44] Previous observational studies found that the frequency of occurrence at low-altitudes [*Bennett et al.*, 1983] and possibly the amplitudes [*Keiling et al.*, 2001] of auroral zone electric fields are controlled by magnetospheric activity. Here, we explore the extent to which the occurrence and amplitudes of the parallel electric fields presented in this study depend on global magnetospheric activity as measured by K_p. Figure 19a shows the distribution of three hour averaged K_p values associated with parallel electric field events. The K_p values range from 0 to 6 with a typical value of 2. Figure 19b shows the distribution of three hour averaged K_p values recorded each time Polar crossed field lines connected to the southern auroral zone over the entire 3-year sampling period. Figure 19c depicts the normalized occurrence pattern determined by dividing the number of parallel electric field events in each K_p bin by the total number of auroral zone crossings registered within that bin over the 3-year period. The estimated errors based on

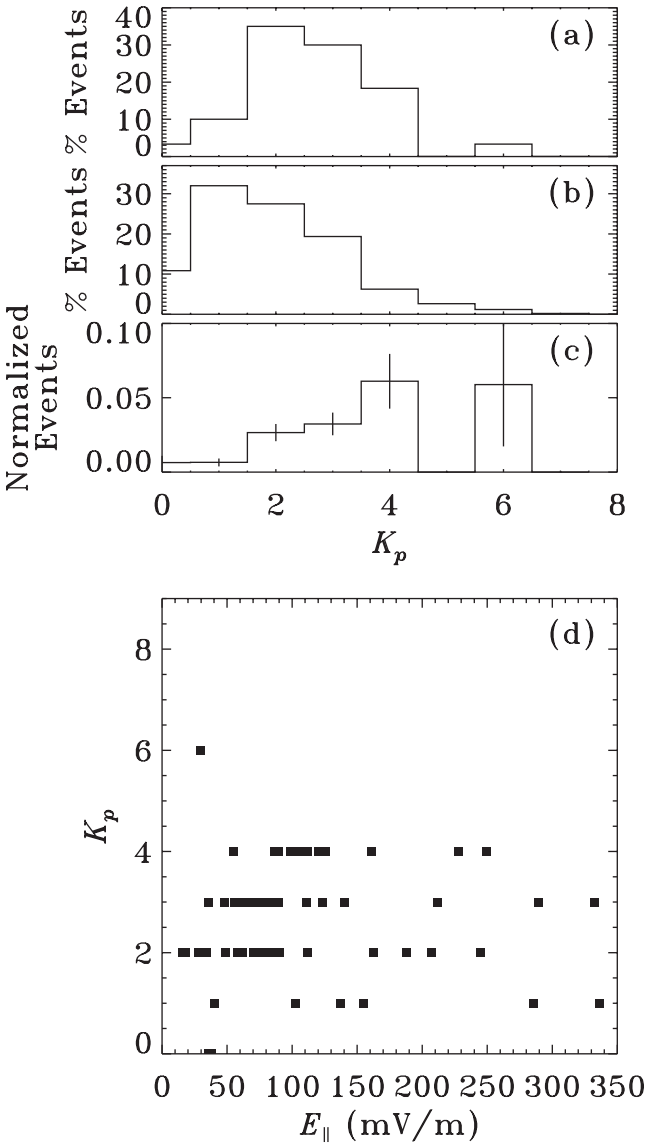

Figure 19. (a) Distribution of three hour averaged K_p values associated with the parallel electric field events, (b) distribution of three hour averaged K_p values recorded each time Polar traversed the southern auroral acceleration region over the 3-year sampling period, (c) normalized occurrence pattern, and (d) comparison of K_p with $E_\parallel$.

Poisson statistics are indicated by vertical bars centered at each K_p bin. Figure 19c shows an increasing frequency of occurrence of parallel electric fields with amplitudes $\geq$25 mV/m with increasing values of K_p between 0 and 4. It is not clear that this trend should continue beyond a $K_p \geq 4$ due to the lack of events at these higher K_p values. The scatterplot displayed in Figure 19d shows no apparent dependence between K_p and $E_\parallel$ amplitudes, except that the $E_\parallel$ events that make up this data set tend to be more commonly associated with less active aurora. The fact that K_p controls the occurrence frequency of large parallel fields, but not the amplitudes, suggests that either the formation of the large parallel electric fields is favored by more active global auroral conditions or that the large parallel fields always exists and that their occurrence at the altitudes sampled by Polar in the southern auroral zone increases with K_p. The second possibility is suggested in the study of auroral zone electric fields with amplitudes $\geq$90 mV/m (shocks) sampled by S3-3 at altitudes between 240 and 8000 km by *Bennett et al.* [1983], which indicated that the shocks tended to occur more frequently at lower altitudes for higher values of K_p.

5. Discussion

[45] The results of the individual case studies together with the statistical results provide important clues to understanding the mechanism or mechanisms that support these large-amplitude, macroscopic parallel electric fields. The statistical results of this paper suggest that the macroscopic parallel electric fields are directed upward and are intimately connected with the maintenance of an upward directed parallel current. The parallel electric fields were shown to be rather localized in space, with typical widths which are of the order of the electron inertial length. The resulting parallel potential has been inferred to extend over roughly tens of kilometers. The tendency for the parallel electric fields to occur at the boundary separating high and low density plasma may be an indication that they occur in response to the plasma's inability to carry the current in the transition between magnetospheric and ionospheric plasmas.

[46] The properties of the parallel electric field are intimately related to the way momentum is imparted to the current carriers, the process of which may depend on effects such as pressure gradients, inertia, and anomalous resistivity as embodied in the generalized Ohm's law. A convenient expression for the steady state electric field that is equivalent to the generalized Ohm's law is the steady state electron momentum equation given by the following expression:

$$\mathbf{E} = -\frac{\mathbf{U_e} \times \mathbf{B}}{c} - \frac{1}{eNe}\nabla \cdot \mathbf{P_e} - \frac{m_e}{e}\mathbf{U_e} \cdot \nabla \mathbf{U_e} + \eta \mathbf{J}, \qquad (1)$$

where m_e is the electron mass, c is the speed of light, e is the electron charge, N_e is the electron density, $\mathbf{U_e}$ is the electron bulk velocity, $\mathbf{P_e}$ is the electron pressure tensor, η is the anomalous resistivity, and $\mathbf{J}$ is the current density. The first term in (1) often denoted the unipolar electric field term has no contributions to the parallel electric field. The second term is the ambipolar electric field term, the third represents electron inertia effects, and the fourth term reflects anomalous resistivity effects, each of which can contribute to $E_\parallel$. Our statistical results show that the parallel field is uncorrelated with the parallel current density. Our statistical results also show a strong anti-correlation between parallel electric field and the logarithm of the density. It is thus fruitful to examine the inertial and ambipolar terms to see if either can reproduce the anti-correlation.

5.1. Electron Inertia

[47] The more or less confinement of $E_\parallel$ and $E_\perp$ to widths which are of the order of the electron inertial length suggests the possibility that inertial effects may be important in supporting the parallel field and establishing its spatial scale. Recent theoretical studies have suggested that electron inertia alone can support the parallel electric fields

responsible for accelerating electrons to keV energies [*Rönnmark*, 1999]. According to *Rönnmark* [1999], the parallel electric field determined by electron inertia can be expressed by the following:

$$E_{\parallel} \sim -\frac{m_e}{e} U_{e\parallel} \frac{\partial U_{e\parallel}}{\partial S_{\parallel}}, \tag{2}$$

where m_e is the electron mass, $U_{e\parallel}$ is the electron bulk speed parallel to the magnetic field vector (which is different from the electron beam speed used to infer the potential from the electron distribution function), and $\partial/\partial\, S_{\parallel}$ is the derivative along the magnetic field. Using the field line conservation constraint $\Gamma = N_e U_{e\parallel}/B = const$ (which is equivalent to $J_{\parallel}/B = const$ along a magnetic flux tube of force if the electrons carry all the current), we can express (2) in terms of gradients in the density and the magnetic field as follows:

$$E_{\parallel} = -\frac{\partial \Phi}{\partial S_{\parallel}} \sim \frac{m_e}{e} \Gamma^2 \left[\frac{B^2}{N_e^3} \frac{\partial N_e}{\partial S_{\parallel}} - \frac{B}{N_e^2} \frac{\partial B}{\partial S_{\parallel}} \right]. \tag{3}$$

The gradients in the plasma density associated with the parallel electric fields are much larger than the magnetic field gradient over the tens of kilometer distances these parallel field occur. This suggests that the first term should dominate yielding an electric field which is in the same direction as the density gradient. The density increases with decreasing altitude. Consequently, the electric field is predicted to point downward, which is contrary to the observations. Thus it appears that the electron inertial effects cannot explain these localized large-amplitude parallel electric fields. However, it is important to mention that such arguments cannot rule out electron inertial effects as a possible explanation for the weak parallel electric fields responsible for kV potential drops distributed over thousands of kilometers at higher altitudes, provided that it can be demonstrated that $|B/\nabla B| > |N_e/\nabla N_e|$.

5.2. Ambipolar Effects

[48] The ambipolar term of the electron momentum equation can support parallel electric fields in regions of sharp density and temperature gradients (e.g., pressure). The present observations are unable to unambiguously determine whether the density gradient along the field line is larger than, smaller than, or of the same order as the temperature gradient. However, the transverse observations inside and outside the density cavities reveal much sharper transitions in the density than in the temperature on the short scales over which the electric fields occur. The electron density outside the cavity, which is dominated by a mixture of ionospheric and magnetospheric components, is much larger than the plasma inside the cavity which is primarily composed of magnetospheric electrons. Typically, the ratios between the density outside and the density inside the cavity were found to be $N_{eI}/N_{eMS} \sim 10$ to 100 and can be as large as 1000 at the altitudes sampled in our study. An examination of the electron temperature changes across these cavities reveals a much weaker transition, namely, the ratio between electron temperature outside to the electron temperature inside was observed (when available) to be roughly $T_{eI}/T_{eMS} \sim 0.3$ to 0.5. Although such a dependence is not necessarily guaranteed along the magnetic field, it is reasonable to assume that the local density gradient along the field line is much larger than that of temperature. In this approximation the parallel electric field can be expressed as

$$E_{\parallel} \approx -\frac{k_b T_e}{e} \frac{\partial \ln(N_e)}{\partial S_{\parallel}}, \tag{4}$$

where k_b is the Boltzmann constant, T_e is the electron temperature, and N_e is the electron density. This formulation of the parallel electric field is equivalent to modeling the electron contribution as a Boltzmann response to the parallel electric field. This expression predicts that the parallel electric field is in the opposite direction of the density gradient. Thus, a downward directed density gradient implies an upward directed parallel electric field which is consistent with our results.

[49] Expression (4) can be rewritten to yield an order of magnitude estimate of the altitudinal extent of the parallel potential as follows:

$$\delta S_{\parallel} \sim \frac{k_b T_e}{e E_{\parallel}} \ln\left(\frac{N_{eI}}{N_{eMS}}\right) \tag{5}$$

Using typical values for electron temperature and the density ratio, (5) yields $\delta S_{\parallel} \sim 20$ to 50 km for a 100 mV/m parallel electric field. This result is in reasonable agreement with the altitudinal extents previously estimated in this study from the measured parallel electric field and parallel potential drop inferred from the electron and ion beam energies.

[50] The typical transverse width of the perpendicular field can also be estimated. For a monotonic potential ramp characteristic of the transverse high and low density transition, the full widths at half maximum of $E_{\perp}$ is in a sense a measure of the perpendicular scale over which the potential drop is distributed. Assuming that the geometry is locally planar and that the ambipolar effects determine the electric field, the parallel length is related to the perpendicular width $W_{E\perp}$ by $\delta S_{\parallel}/W_{E\perp} = 1/\epsilon$. Thus, we obtain an expression for the perpendicular width of the following form:

$$W_{E\perp} \sim \epsilon \frac{k_b T_e}{e E_{\parallel}} \ln\left(\frac{N_{eI}}{N_{eMS}}\right) \tag{6}$$

Using the peak value for $\epsilon \sim 0.4$ yields $W_{E\perp} \sim 8$ for a density ratio of 10 and a 1 keV electron temperature. This compares favorably with the median value of $W_{E\perp}$ which was found to be 6 km.

[51] Finally, the statistical anticorrelation between the parallel electric field and the plasma density can be explained by the following heuristic arguments. If on average the parallel electric field measurements were taken near the center of the parallel potential ramp, the density can be approximated as $\ln N^* \approx (\ln N_I + \ln N_{MS})/2$. Substituting this into (5), we get a relation between the parallel electric field and the locally measured density as follows: $E_{\parallel}^* \approx -2(k_b T_e/e)[\ln N^* - \ln N_I]/\delta S_{\parallel}$. Thus, with all other things being equal for different events, a smaller value of N^* will give rise to a larger $E_{\parallel}^*$. This expression is just approximate, and breaks down when Polar is traversing the parallel electric field region near the top or bottom of the region. Physically, the statistical anticorrelation is

viewed as a manifestation of an ambipolar parallel electric field, the strength of which depends on the sharpness of the density transition along the field-line.

[52] These results suggest that the ambipolar term of the generalized Ohm's law provides a feasible explanation for both the parallel and perpendicular electric field structures associated with the sharp density transitions. However, an unambiguous judgment would require measurements along the magnetic field. Not precluded from this analysis is the possibility that the parallel potential associated with these large-amplitude fields are the results of significant violations of quasineutrality (e.g., a sheath effect) often observed in experimental devices and considered in several theoretical studies. The parallel electric field amplitude is likely to be a lower bound on the maximum field that can occur along the field line. Much larger fields can occur along the field line characteristic of a sheath potential as suggested in more recent observational [*Mozer and Hull*, 2001] and theoretical models [*Ergun et al.*, 2000]. It may be the case that the parallel electric fields discussed in this study are characteristic of a presheath (a region where the quasineutral approximation is valid).

6. Conclusions

[53] This paper presents the first statistical study of large-amplitude, macroscopic parallel electric fields in the upward current portion of the southern auroral zone at altitudes ranging from $0.8R_E$ to $1.5R_E$. We found 64 events characterized by $E_{\|}$ ranging in amplitude from about 25 to 300 mV/m. Moreover, $E_{\|}$ represents a significant fraction of the total electric field strength (the $E_{\|}/E_{\perp}$ ratios range from $\sim$0.25 to O(10)). Many of the parallel electric field structures occur at the edges of converging pairs of perpendicular electric field structures (electrostatic shocks). The $E_{\|}$ structures are associated with the upward current, tending to occur within or near regions containing upgoing ions and downgoing electrons. The large-amplitude parallel electric fields tend to occur preferentially within a thin layer centered about $1.28R_E$. In addition, the occurrence of these large-amplitude parallel electric fields increases with increasing values of K_p between 0 and 4. It is not clear that this tendency should continue for higher K_p values due to the low statistics. We find no apparent correlation between the magnitude of $E_{\|}$ and altitude, current, and K_p, although there is a suggestion that the largest $E_{\|}/E_{\perp}$ ratios are confined to lower altitudes. The large parallel electric fields imply significant parallel potential drops that are rather localized in altitude (e.g., tens of kilometers as opposed to $\sim$ thousands of kilometers). The $E_{\|}$ structures have spatial widths that range from $\sim$1.0 to 20 km which map to 100 m to 2 km at ionospheric altitudes, with a distribution that is in rough correspondence with the distribution that characterizes the smallest scale sizes of discrete auroral arcs [e.g., *Maggs and Davis*, 1968]. Thus, the observed $E_{\|}$ could be a source of small-scale auroral structures embedded in broad arcs. The spatial widths that characterize the $E_{\|}$ signatures are typically of the order of the electron inertial length. We tested the kinetic wave expectation of the parallel and perpendicular fields and demonstrated that at least for the example tested the explanation does not appear to be feasible. A detailed analysis suggests that these large-amplitude parallel electric fields are probably the result of an ambipolar response of the plasma to sharp gradients in density at the interface separating the cold, dense ionospheric plasma from the hot, tenuous magnetospheric plasma.

[54] **Acknowledgments.** We thank C. T. Russell for the generous free use of the Polar magnetometer data. A. J. H. wishes to thank C. Chaston for useful discussions. The work at UC Berkeley was supported by NASA grant 5-3182. Partial support for this work for J. D. S. from NASA grant 5-7883 is also acknowledged.

References

Bennett, E. L., M. Temerin, and F. S. Mozer, The distribution of auroral electrostatic shocks below 8000-km altitude, *J. Geophys. Res.*, *88*, 7107–7120, 1983.

Boehm, M. H., C. W. Carlson, J. P. McFadden, J. H. Clemmons, R. E. Ergun, and F. S. Mozer, Wave rectification in plasma sheaths surrounding electric field antennas, *J. Geophys. Res.*, *99*, 21,361–31,374, 1994.

Cattell, C. A., F. S. Mozer, I. Roth, R. R. Anderson, R. C. Elphic, W. Lennartsson, and E. Ungstrup, ISEE 1 observations of electrostatic ion cyclotron waves in association with ion beams on auroral field lines from $\sim$2.5 to 4.5 R_E, *J. Geophys. Res.*, *96*, 11,421–11,439, 1991.

Cattell, C., et al., The association of electrostatic ion cyclotron waves, ion and electron beams and field-aligned currents: FAST observations of an auroral zone crossing near midnight, *Geophys. Res. Lett.*, *25*, 2053–2056, 1998a.

Cattell, C. A., J. R. Wygant, J. Dombeck, F. S. Mozer, M. A. Temerin, and C. T. Russell, Observations of large amplitude parallel electric field wave packets at the plasma sheet boundary, *Geophys. Res. Lett.*, *25*, 857–860, 1998b.

Cattell, C. A., et al., Comparisons of Polar satellite observations of solitary wave velocities in the plasma sheet boundary and the high altitude cusp to those in the auroral zone, *Geophys. Res. Lett.*, *26*, 425–428, 1999.

Ergun, R. E., et al., FAST satellite observations of electric field structures in the auroral zone, *Geophys. Res. Lett.*, *25*, 2025–2028, 1998a.

Ergun, R. E., et al., FAST satellite observations large-amplitude solitary structures, *Geophys. Res. Lett.*, *25*, 2041–2044, 1998b.

Ergun, R. E., C. W. Carlson, J. P. McFadden, F. S. Mozer, and R. J. Strangeway, Parallel electric fields in discrete arcs, *Geophys. Res. Lett.*, *27*, 4053–4056, 2000.

Ergun, R. E., Y. J. Su, L. Andersson, C. W. Carlson, J. P. McFadden, F. S. Mozer, D. L. Newman, M. V. Goldman, and R. J. Strangeway, Direct observations of localized parallel electric fields in a space plasma, *Phys. Rev. Lett.*, *87*, 5003, 2001.

Gorney, D. J., A. Clarke, D. Croley, J. Fennell, J. Luhman, and P. Mizera, The distribution of ion beams and conics below 8000 km, *J. Geophys. Res.*, *86*, 83–89, 1981.

Gurnett, D. A., et al., The Polar plasma wave instrument, *Space Sci. Rev.*, *71*, 597–622, 1995.

Harvey, P., et al., The electric field instrument on the Polar satellite, *Space Sci. Rev.*, *71*, 583–596, 1995.

Keiling, A., J. R. Wygant, C. A. Cattell, M. Johnson, M. Temerin, F. S. Mozer, C. A. Kletzing, J. Scudder, and C. T. Russell, Properties of large electric fields in the plasma sheet at 4–7 r_e measured with Polar, *J. Geophys. Res.*, *106*, 5779–5798, 2001.

Kintner, P. M., M. C. Kelley, R. D. Sharp, A. G. Ghielmetti, M. Temerin, C. Cattell, and J. F. Fennell, Simultaneous observations of energetic (keV) upstreaming ions and electrostatic hydrogen cyclotron waves, *J. Geophys. Res.*, *84*, 7201–7212, 1979.

Knight, S., Parallel electric fields, *Planet. Space Sci.*, *21*, 741–750, 1973.

Lin, C. S., and R. A. Hoffman, Characteristics of the inverted-V event, *J. Geophys. Res.*, *84*, 1514–1524, 1979.

Lysak, R. L., The relationship between electrostatic shocks and kinetic Alfvén waves, *Geophys. Res. Lett.*, *25*, 2089–2092, 1998.

Lysak, R. L., and W. Lotko, On the dispersion relation for shear Alfvén waves, *J. Geophys. Res.*, *101*, 5085–5094, 1996.

Maggs, J. E., and T. N. Davis, Measurements of the thickness of auroral structures, *Planet. Space Sci.*, *16*, 205–209, 1968.

Mozer, F. S., On the lowest altitude S3-3 observations of electrostatic shocks and parallel electric fields, *Geophys. Res. Lett.*, *7*, 1097–1098, 1980.

Mozer, F. S., ISEE 1 observations of electrostatic shocks on auroral zone field lines between 2.5 and 7 Earth radii, *Geophys. Res. Lett.*, *7*, 823–826, 1981.

Mozer, F. S., and A. Hull, The origin and geometry of upward parallel electric fields in the auroral acceleration region, *J. Geophys. Res.*, *106*, 5763, 2001.

Mozer, F. S., and C. A. Kletzing, Direct observation of large, quasi-static,

parallel electric fields in the auroral acceleration region, *Geophys. Res. Lett.*, *25*, 1629–1632, 1998.

Mozer, F. S., C. W. Carlson, M. K. Hudson, R. B. Torbert, B. Parady, J. Yatteau, and M. C. Kelley, Observations of paired electrostatic shocks in the polar magnetosphere, *Phys. Rev. Lett.*, *38*, 292–295, 1977.

Mozer, F. S., C. A. Cattell, M. K. Hudson, R. L. Lysak, M. Temerin, and R. B. Torbert, Satellite measurements and theories of low altitude auroral particle acceleration, *Space Sci. Rev.*, *27*, 155–213, 1980.

Redsun, M. S., M. Temerin, and F. S. Mozer, Classification of auroral electrostatic shocks by their ion and electron associations, *J. Geophys. Res.*, *90*, 9615–9633, 1985.

Rönnmark, K., Electron acceleration in the auroral current circuit, *Geophys. Res. Lett.*, *26*, 983–986, 1999.

Russell, C. T., R. C. Snare, J. D. Means, D. Pierce, D. Dearborn, M. Larson, G. Barr, and G. Le, The GGS/Polar magnetic fields investigation, *Space Sci. Rev.*, *71*, 563–582, 1995.

Scudder, J., et al., Hydra - a three-dimensional electron and ion hot plasma instrument for the Polar spacecraft of the GGS mission, *Space Sci. Rev.*, *71*, 459–495, 1995.

Scudder, J. D., X. Cao, and F. S. Mozer, Photoemission current-spacecraft voltage relation: Key to routine, quantitative low-energy plasma measurements, *J. Geophys. Res.*, *105*, 21,281–21,294, 2000.

Stasiewicz, K., et al., Small scale Alfvénic structure in the aurora, *Space Sci. Rev.*, *92*, 423–533, 2000.

Temerin, M., K. Cerny, W. Lotko, and F. S. Mozer, Observations of double layers and solitary waves in the auroral plasma, *Phys. Rev. Lett.*, *48*, 1175–1179, 1982.

Torrence, C., and G. P. Compo, A practical guide to wavelet analysis, *Bull. Am. Meteorol. Soc.*, *79*, 61–78, 1998.

J. W. Bonnell, A. J. Hull, and F. S. Mozer, Space Science Laboratory, University of California, Berkeley, CA 94720, USA. (ahull@ssl.berkeley.edu)

J. D. Scudder, Department of Physics and Astronomy, University of Iowa, Iowa City, IA 52242, USA.